Cellular/Molecular

Regulated Dynamic Trafficking of Neurexins Inside and Outside of Synaptic Terminals

Christian Neupert,[1]* Romy Schneider,[2]* Oliver Klatt,[1,2] Carsten Reissner,[1] Daniele Repetto,[1] Barbara Biermann,[1,2] Katharina Niesmann,[1] Markus Missler,[1,3] and Martin Heine[2,4]

[1]Institute of Anatomy and Molecular Neurobiology, Westfälische Wilhelms-University, 48149 Münster, Germany, [2]Molecular Physiology Group, Leibniz-Institute of Neurobiology, 39118 Magdeburg, Germany, [3]Cluster of Excellence EXC 1003, Cells in Motion, 48149 Münster, Germany, and [4]Center for Behavioral Brain Sciences, 39118 Magdeburg, Germany

Synapses depend on trafficking of key membrane proteins by lateral diffusion from surface populations and by exocytosis from intracellular pools. The cell adhesion molecule neurexin (Nrxn) plays essential roles in synapses, but the dynamics and regulation of its trafficking are unknown. Here, we performed single-particle tracking and live imaging of transfected, epitope-tagged Nrxn variants in cultured rat and mouse wild-type or knock-out neurons. We observed that structurally larger αNrxn molecules are more mobile in the plasma membrane than smaller βNrxns because αNrxns displayed higher diffusion coefficients in extrasynaptic regions and excitatory or inhibitory terminals. We found that well characterized interactions with extracellular binding partners regulate the surface mobility of Nrxns. Binding to neurexophilin-1 (Nxph1) reduced the surface diffusion of αNrxns when both molecules were coexpressed. Conversely, impeding other interactions by insertion of splice sequence #4 or removal of extracellular Ca^{2+} augmented the mobility of αNrxns and βNrxns. We also determined that fast axonal transport delivers Nrxns to the neuronal surface because Nrxns comigrate as cargo on synaptic vesicle protein transport vesicles (STVs). Unlike surface mobility, intracellular transport of βNrxn$^+$ STVs was faster than that of αNrxns, but both depended on the microtubule motor protein KIF1A and neuronal activity regulated the velocity. Large spontaneous fusion of Nrxn$^+$ STVs occurred simultaneously with synaptophysin on axonal membranes mostly outside of active presynaptic terminals. Surface Nrxns enriched at synaptic terminals where αNrxns and Nxph1/αNrxns recruited $GABA_AR$ subunits. Therefore, our results identify regulated dynamic trafficking as an important property of Nrxns that corroborates their function at synapses.

Key words: autism; GABA(A) receptors; imaging; neuroligin; quantum dots; synapse function

Significance Statement

Synapses mediate most functions in our brains and depend on the precise and timely delivery of key molecules throughout life. Neurexins (Nrxns) are essential synaptic cell adhesion molecules that are involved in synaptic transmission and differentiation of synaptic contacts. In addition, Nrxns have been linked to neuropsychiatric diseases such as autism. Because little is known about the dynamic aspects of trafficking of neurexins to synapses, we investigated this important question using single-molecule tracking and time-lapse imaging. We identify distinct differences between major Nrxn variants both in surface mobility and during intracellular transport. Because their dynamic behavior is highly regulated, for example, by different binding activities, these processes have immediate consequences for the function of Nrxns at synapses.

Introduction

Synapse differentiation and plasticity are fast and highly regulated processes that require the coordinated targeting of a plethora of specialized molecules to presynaptic and postsynaptic compartments (McAllister, 2007; Chia et al., 2013). Presynaptic proteins can be delivered from intracellular pools via synaptic vesicle protein transport vesicles (STVs), piccolo-bassoon transport vesicles (PTVs), or dense-core vesicles (DCVs; Ahmari et al., 2000; Zhai et al., 2001; Sabo et al., 2006; de Wit et al., 2009a; Bury and Sabo, 2011; Park et al., 2011; van de Bospoort et al., 2012). In

Received Sept. 30, 2014; revised Aug. 26, 2015; accepted Aug. 26, 2015.

Author contributions: C.N., M.M., and M.H. designed research; C.N., R.S., O.K., C.R., D.R., B.B., and M.H. performed research; C.R. and K.N. contributed unpublished reagents/analytic tools; C.N., R.S., O.K., C.R., D.R., B.B., M.M., and M.H. analyzed data; M.M. and M.H. wrote the paper.

This work was supported by Deutsche Forschungsgemeinschaft (Grant SFB629-TPB11 to M.M. and Grant HE3604/2-1 to M.H.), and Land Sachsen-Anhalt (LSA Research Group Molecular Physiology Grant to M.H.). We thank K. Kerkhoff, S. Opitz, A. Lenuweit, H. Wickborn, and I. Wolff for excellent technical assistance; M. Klose for biochemical experiments during early stages of the project; and J. Klingauf (Biophysics, Münster) and members of our laboratories for discussion.

The authors declare no competing financial interests.

*C.N. and R.S. contributed equally to this work.

addition, synaptic membrane proteins can be distributed by lateral diffusion of surface populations (Ribrault et al., 2011; Chang et al., 2012; Cijsouw et al., 2014; Schneider et al., 2015). Because neurotransmission differs between synapses even of the same neuron (Rozov et al., 2001; Ermolyuk et al., 2012), regulated trafficking of synaptic components contributes to their functional specification (Lau and Zukin, 2007; Vithlani et al., 2011; Anggono and Huganir, 2012; Dolphin, 2012; Chia et al., 2013). The molecular determinants controlling the shaping of synapses with different properties are incompletely understood, but it was hypothesized that the transmembrane proteins neurexins (Nrxns) in concert with binding partners play a role (Shen and Scheiffele, 2010; Missler et al., 2012; Reissner et al., 2013). Little is known about the trafficking of Nrxn to synapses except the requirement of the C-terminal PDZ-recognition motif to traverse the secretory pathway (Fairless et al., 2008; Gokce and Südhof, 2013).

Several findings render Nrxns as candidates for the organization of synaptic function. Nrxns represent a polymorphic family of differentially distributed, alternatively spliced molecules (Ullrich et al., 1995; Schreiner et al., 2014; Treutlein et al., 2014), for which an increasing number of binding partners provide extracellular cues (Ichtchenko et al., 1995; Missler et al., 1998; Sugita et al., 2001; Boucard et al., 2005; Ko et al., 2009; de Wit et al., 2009b; Uemura et al., 2010; Matsuda and Yuzaki, 2011; Boucard et al., 2012; Reissner et al., 2014). Both α-neurexin (αNrxn), with its large extracellular domain, and the shorter β-neurexin (βNrxn) are able to differentiate synapses *in vitro* (Dean et al., 2003; Graf et al., 2004; Nam and Chen, 2005). αNrxns are functionally essential for synaptic transmission at excitatory and inhibitory terminals in many brain areas (Missler et al., 2003; Kattenstroth et al., 2004; Zhang et al., 2005; Etherton et al., 2009; Zhang et al., 2010; Bottos et al., 2011; Aoto et al., 2013). βNrxn have less impact on neurotransmission (Born et al., 2015), consistent with their lower abundance (Schreiner et al., 2015). Finally, together with binding partners, presynaptic Nrxns affect the function of postsynaptic ion channels (Kattenstroth et al., 2004; Heine et al., 2008a; Zhang et al., 2010; Mondin et al., 2011; Aoto et al., 2013; Budreck et al., 2013; Giannone et al., 2013; Born et al., 2014; Born et al., 2015).

In contrast to the established importance of the dynamic trafficking of ion channels (Heine et al., 2008b; Bannai et al., 2009; Dupuis et al., 2014), cell-adhesion molecules as Nrxn often invoke the idea of engaging in relatively immobile *trans*-synaptic contacts. However, an earlier study predicted from population measurements of pHluorin-tagged Nrxns that their mobility is pertinent to GABAergic synapse maintenance in parvalbumin interneurons (Fu and Huang, 2010). Because most synapses can undergo rapid plasticity (Dobie and Craig, 2011; Kwon and Sabatini, 2011; Chen et al., 2012), here, we investigated the dynamic trafficking of Nrxns outside and inside of synapses. Because nonperturbing antibodies against endogenous Nrxn variants are not available, we relied on overexpression of epitope-tagged proteins. Previous work demonstrated that peroxidase-tagged αNrxn partially rescues the release phenotype of knock-out mice (Missler et al., 2003; Zhang et al., 2005), and that fluorochrome-tagged Nrxn shows synaptic targeting independent of endogenous protein (Fairless et al., 2008; Gokce and Südhof, 2013). Using single-particle tracking (SPT) and time-lapse imaging of epitope-tagged αNrxn and βNrxn variants, we now reveal their distinct and highly regulated dynamic behavior at the surface and intracellularly.

Materials and Methods

Animals. Rat and mouse pups of either sex were used for primary hippocampal culture and derived from timed-pregnant dams at embryonic day 18 (E18; rats) or E17 (mice). Generation and genotyping of αNrxn-deficient mice has been described previously (Missler et al., 2003). All experiments were performed in accordance with local institutional and government regulations for animal welfare at the Leibniz Institute of Neurobiology (Magdeburg, Germany) under license 53.23-42500 and at University of Münster approved by the Landesamt für Natur, Umwelt und Verbraucherschutz, North Rhine-Westphalia under license 84-02.05.20.11.209.

Antibodies. Primary antibodies were as follows: monoclonal mouse antibody against the lumenal domain of synaptotagmin1, CypHer5E-labeled (SynapticSystems; catalog #105311CpH), polyclonal rabbit Oyster 550-labeled antibody against the luminal domain of synaptotagmin1 (SynapticSystems; catalog #105103C3), polyclonal rabbit oyster 550-labeled antibody against the luminal domain of VGAT (SynapticSystems; catalog #131103C3), polyconal guinea pig against VGluT1 (SynapticSystems; catalog #135304), polyclonal rabbit antibody (serum) against GFP (Life Technologies; catalog #A-6455), monoclonal mouse antibody against GFP (Roche; catalog #11814460001), GFP-Booster Atto 488 (ChromoTek; catalog #gba488), polyclonal guinea pig antibody against bassoon (SynapticSystems; catalog #141004), polyclonal rabbit antibody against KIF1A (Sigma-Aldrich; catalog #SAB2104191), polyclonal rabbit antibody against NEEP21 (Santa Cruz Biotechnology; catalog #sc-135089), polyclonal rabbit antibody against Rab3a (Sigma-Aldrich; catalog #R2776), polyclonal rabbit antibody against Rab5a (Sigma-Aldrich; catalog #R4654), monoclonal mouse antibody against Rab7b (Sigma-Aldrich; catalog #WH0338382M1), monoclonal mouse antibody against Rab11 (Abcam; catalog #AB78337), monoclonal mouse antibody against Tubulin (SynapticSystems; catalog #302211), monoclonal mouse antibody against CASK (Millipore; catalog #MAB5230), polyclonal rabbit antibodies against Rim1α and Mint1 (gift from T.C. Südhof, Stanford University), and quantum dot 655 anti-mouse (QD-655; Life Technologies; catalog #Q11022MP). Secondary antibodies were as follows: Alexa Fluor488 goat-anti-rabbit, Alexa Fluor488 goat-anti-mouse IgG (Invitrogen), Cy3-conjugated goat-anti-rabbit, and Cy3-conjugated goat-anti-mouse IgG (Jackson Immuno Research).

Neuronal cultures. Primary neurons were prepared in HBSS from hippocampi of E17 mice or E18 rats as described previously (Kaech and Banker, 2006). Briefly, cell suspensions obtained after 0.25% trypsin treatment and trituration were plated onto 18 mm glass coverslips (Menzel-Glaeser) coated with poly-L-lysine (Sigma-Aldrich) at a density of 20,000 cells per coverslip. After 1–2 h at 37°C, 5 coverslips were transferred into a 35 mm dish containing a 70–80% confluent monolayer of astrocytes in neurobasal medium supplemented with B27 and 5 mM glutamine. Cultures were maintained at 37°C in a humidified incubator with an atmosphere of 95% air and 5% CO_2. Neurons were transfected at 4–6 days *in vitro* (DIV) using calcium phosphate, effectene (Qiagen), or lipofectamine (Life Technologies) and experiments were performed between DIV7 and DIV10 (intracellular transport) or DIV14 and DIV21 (surface mobility, pHluorin). For live imaging experiments, dissociated neurons were seeded onto poly-L-lysin-coated dishes (ibidi) at low density (50–100 cells/mm^2) and cultured with a layer of astrocytes on a coverslip.

Expression vectors and reagents. pSyn5-Nrxn vectors were cloned from earlier variants (Fairless et al., 2008) by replacing CMV with a human synapsin promoter to obtain pSyn5-NENA (EGFP fused at the N terminus of Nrxn1α) and pSyn5-NENB (for Nrxn1β). mCherry from pCDNA3.1/hChR2-mCherry replaced EGFP in pSyn5-EchNA and pSyn5-EchNB using oligonucleotide primers MM08-60 (forward, 5′-CGA CGA GCT AGC AAG CTT ATG GTG AGC AAG GGC GAG GAG

Correspondence should be addressed to either of the following: Markus Missler, Institute of Anatomy and Molecular Neurobiology, Westfälische Wilhelms-University, Vesaliusweg 2-4, Münster 48149, Germany, E-mail:: Markus.Missler@uni-muenster.de; or Martin Heine, Molecular Physiology Group, Leibniz-Institute of Neurobiology, Brenneckestrasse 6, 39118 Magdeburg, Germany, E-mail: Martin.Heine@ifn-magdeburg.de.

DOI:10.1523/JNEUROSCI.4041-14.2015

Copyright © 2015 the authors 0270-6474/15/3513630-19$15.00/0

G-3′) and MM08–30 (reverse, 5′-CGA CGA GCT AGC CTT GTA CAG CTC GTC CAT GCC-3′). For pH-sensitive vectors, a super ecliptic pHluorin was amplified from synapto-pHluorin (provided by Jürgen Klingauf, Münster University, Germany) and inserted in pSyn5-NpHNA and pSyn5-NpHNB (SEP_Nrxn1α and SEP_Nrxn1β with SEP at N terminus). Oligonucleotide primers MM09–107 (forward, 5′-CGA CGA GCT AGC GGA GCA GGA ATG AGT AAA GGA GAA GAA CTT TTC ACT GG-3′) and MM09–108 (reverse, 5′-CGA CGA GCT AGC TCC TGC TCC ACC GGT TTT GTA TAG TTC ATC CAT GCC ATG-3′) yielded pHluorin with overhangs containing NheI sites (5′ and 3′), and an *Age*I site (3′) to test orientation. For pSyn-Nxph1Cterm-pH [neurexophilin-1 ((Nxph1) with SEP at C terminus], the SEP sequence was amplified using primers MM10–61 (forward, 5′-CGA CGA CCC GGG AGT AAA GGA GAA GAA CTT TTC ACT GGA GTT GTC CCA ATT CTT GTT GAA TTA GAT GGT GAT GTT AAT GG-3′) and MM10–62 (reverse, 5′-CGA CGA CCC GGG TCA TTT GTA TAG TTC ATC CAT GCC ATG TGT AAT CCC AGC AGC-3′), yielding pHluorin with XmaI sites. Synaptophysin with pHTomato and HA tags in pSyn5 were generated from pQUAS-Synaptophysin-pHTomato-sv40 (provided by J.Klingauf) via NotI-XbaI sites. For Ca^{2+} imaging, pGP-CMV-GCaMP6f (Addgene) was used.

EGFP-KIF1A plasmid (Lee et al., 2003) was kindly provided by Jae-Ran Lee (Korea Advanced Institute of Science and Technology, Daejeon, South Korea), EGFP-KIF1A-shRNA (Liu et al., 2012) and shRNA-resistant myc-KIF1A (Xue et al., 2010) constructs were generously provided by Judy S. Liu (Center for Neuroscience Research, Children's National Medical Center, Washington, DC). All enzymes for restriction site digest, dephosphorylation, ligation, and appropriate buffers were purchased from New England Biolabs. Primers were generated by Sigma-Aldrich and PCRs performed with the Expand Long Template PCR kit (Roche Applied Science). DNA fragments were isolated using a standard phenol-chloroform extraction protocol or from agarose gels with a QiaEx kit (Qiagen). All resulting intermediaries and final constructs were confirmed by DNA sequencing.

Time-lapse imaging. To monitor intracellular transport, cultures were placed in HEPES buffer containing the following (in mM): 145 NaCl, 2.5 KCl, 2 $CaCl_2$, 2 $MgCl_2$, 10 Glucose, 10 HEPES, pH 7.4. Cultures were then observed with a spinning disc Axio Observer-Z1 (Visitron) with a dual CCD-camera Orca-D2 (Hamamatsu Photonics) and an EMCCD camera (ImagEM 512 CCD; Hamamatsu) using a 40× Plan-Neofluar oil-immersion objective and heated stage (36°C). Time-lapse recordings for up to 10 min with intervals of 100–500 ms were acquired to analyze vesicle trafficking. Vesicles that never moved were excluded. Trajectories and velocities of moving vesicles were determined via kymograph function in MetaMorph (Molecular Devices). A period was considered mobile when it displayed movement faster than 0 ± 0.10 μm/s. Axons and dendrites were distinguished based on their morphological characteristics. Disruption of cytoskeletal elements was achieved by 5 μM latrunculin-A and 10 μM nocodazole (both from Sigma-Aldrich). Neuronal activity experiments were performed with 1 μM TTX (Alomone Labs) and depolarizing HEPES buffer containing the following (in mM): 61.5 NaCl, 60 KCl, 2 $CaCl_2$, 2 $MgCl_2$, 30 Glucose, and 25 HEPES, pH 7.4. Electrical field stimulation of neuronal cultures transfected with GCamp6f was applied with parallel platinum electrodes and an isolated pulse generator 2100 (AM Systems) in combination with a stimulus isolator (A385; World Precision Instruments) delivering 52 mA pulses of 1 ms duration. The stimulus used was 1–16 trains of 50 APs at 50 Hz with 5 s interval.

Immunocytochemistry. Neurons were fixed in 4% PFA/PBS for 10 min at room temperature, permeabilized in 0.3% Triton X-100, and blocked in 2% BSA/25 mM glycine or 5% normal goat serum/PBS. Primary and secondary antibodies were diluted in blocking buffer and F-actin was visualized by incubating with Alexa Fluor 488- or Alexa Fluor 568-phalloidin (1:100; Invitrogen). Images were taken with epifluorescent microscopes (Zeiss; Imager A2 or Axio Imager.Z2) equipped with a 63× 1.4 numerical aperture (NA) Plan-Apochromat objectives and CCD cameras (CoolSnap EZ, Roper-Scientific, or Spot Xplorer and apotome Visitron).

Fluorescent recovery after photo bleach. For fluorescent recovery after photo bleach (FRAP), primary neurons transfected with pHluorin-tagged plasmids were perfused with solution containing the following (in mM): 145 NaCl, 2.5 KCl, 2 $MgCl_2$, 2 $CaCl_2$, 10 HEPES, and 10 D-glucose, pH 7.4. For low pH, HEPES was replaced by MOPS, pH 5.5. A rapid solution exchange using a theta-glass electrode with low pH-solution in one and extracellular solution containing the following (in mM): 50 NH_4Cl 95 NaCl, 2.5 KCl, 2 $MgCl_2$, 2 $CaCl_2$, 10 HEPES, and 10 D-glucose, pH 7.4, was used in the other channel-determined fluorescent ratios. Fluorescence was excited using a mercury lamp (DG4; Sutter Instruments) controlled by MetaMorph software (Universal Imaging). To photobleach locally, a diode laser 473 nm/80 mW (Rapp OptoElectronic) was used at 50–100% power with a spot illumination time of 10–20 ms. The laser was coupled to the microscope via a galvometric mirror guided by a UGA 40 control unit (Rapp OptoElectronic), which allowed us to photobleach several regions within a short time window (<200 ms). FRAP was monitored at 10 Hz and recovery curves were corrected for background noise.

Single-particle tracking. EGFP or pHluorin-tagged proteins were labeled either with QD-655 bound to monoclonal anti-GFP and anti-Flag antibodies (Roche; catalog #11814460001) or nanobodies against GFP (Muyldermans, 2013) conjugated to ATTO 647N (Chromotek; catalog #gba647N). QD-655 and goat F(ab′)2 anti-mouse IgG conjugate (H+L) highly cross-adsorbed (0.1 μM; Life Technologies; catalog #Q-11021MP) were precoated with mouse anti-GFP (0.5 μg) in 10 μl of PBS for 30 min and blocked with casein for 15 min. Transfected neurons were incubated with 0.1–0.01 nM QDs for 1–5 min at 37°C, washed in HEPES-buffered physiological solution containing the following (in mM): 145 NaCl, 2.5 KCl, 2 $MgCl_2$, 2 $CaCl_2$, 10 HEPES, and 10 D-glucose, pH 7.4, plus 0.5% BSA, transferred to an open chamber, and imaged. In case of nanobody labeling, cultures were mounted in a Ludin chamber (Life Imaging Services) and anti-GFP nanobodies were applied to the media in a dilution of 1:50,000. The high dilution ensured separation of individual molecules and the reduction of background fluorescence from unbound nanobodies. To visualize active synapses (Kraszewski et al., 1995; Martens et al., 2008), the uptake of fluorophore-coupled antibodies against the luminal domain of synaptotagmin1 (1:200, precoupled to CypHer5E, SynSys) or VGAT (1:200, Oyster550, SynSys) was used before QD or nanobody labeling. Recordings of anti-GFP QDs labeled GFP-Nrxn relative to synaptotagmin1 or VGAT clusters were conducted with an AxioObserver microscope (Zeiss) equipped with an EMCCD camera (Evolve; Roper Photometrics) using a 100× 1.3 NA objective or at a spinning disc Axio Observer-Z1 (Visitron) equipped with an EMCCD camera (ImagEM C9100-13; Hamamatsu) using a 100 × 1.46 NA Plan-Apochromat oil-immersion objective (Zeiss). Fluorescence of QDs and presynaptic markers was excited with a xenon lamp using excitation filters HC 435/40, HC 531/40, and ET 640/30 (Semrock/Chroma) or with a 561 nm Laser (100 mW; Visitron). Emitted fluorescence was acquired through filters HC 593/40, HC 655/15, and ET Bandpass 690/50, respectively. Recordings of QDs were obtained with an integration time of 30 ms for up to 1000–2000 consecutive frames. QD-labeled Nrxns were followed on randomly selected dendritic regions for up to 20 min. QD fixed to the coverslip allowed to compensate for mechanical drifts of the stage. Nanobody-labeled Nrxns were imaged with an inverted fluorescent microscope (Olympus IX71) with TIRF illumination, a high-magnification objective (100× NA 1.49), and EMCCD camera (iXON Ultra; Andore). The laser illumination (630 nm, 100 mW) was adjusted to have oblique illumination using 10–20% of the laser power. The acquisition rate was 50 Hz with a localization accuracy similar to QD-based SPT (<50 nm). All recordings of molecular mobility were performed at 36–37°C.

Tracking analysis. Single QDs were tracked using custom-made software (Groc et al., 2007). Trajectories of single QDs were reconstructed with a point accuracy of 50–60 nm and subtrajectories reconnected when the displacement between 2 frames was 1–2 pixels (maximal dark period of 25 frames). For motion parameters of single molecules, mean squared displacement (MSD) curves were calculated and plotted over time for reconnected trajectories of at least 100 frames (resolution limit for diffusion was 0.001 μm^2/s). Diffusion coefficients were calculated by linear fit of the first four points of the MSD plots versus time (Saxton, 1995). The diffusion coefficient, confinement index, and dwell time were

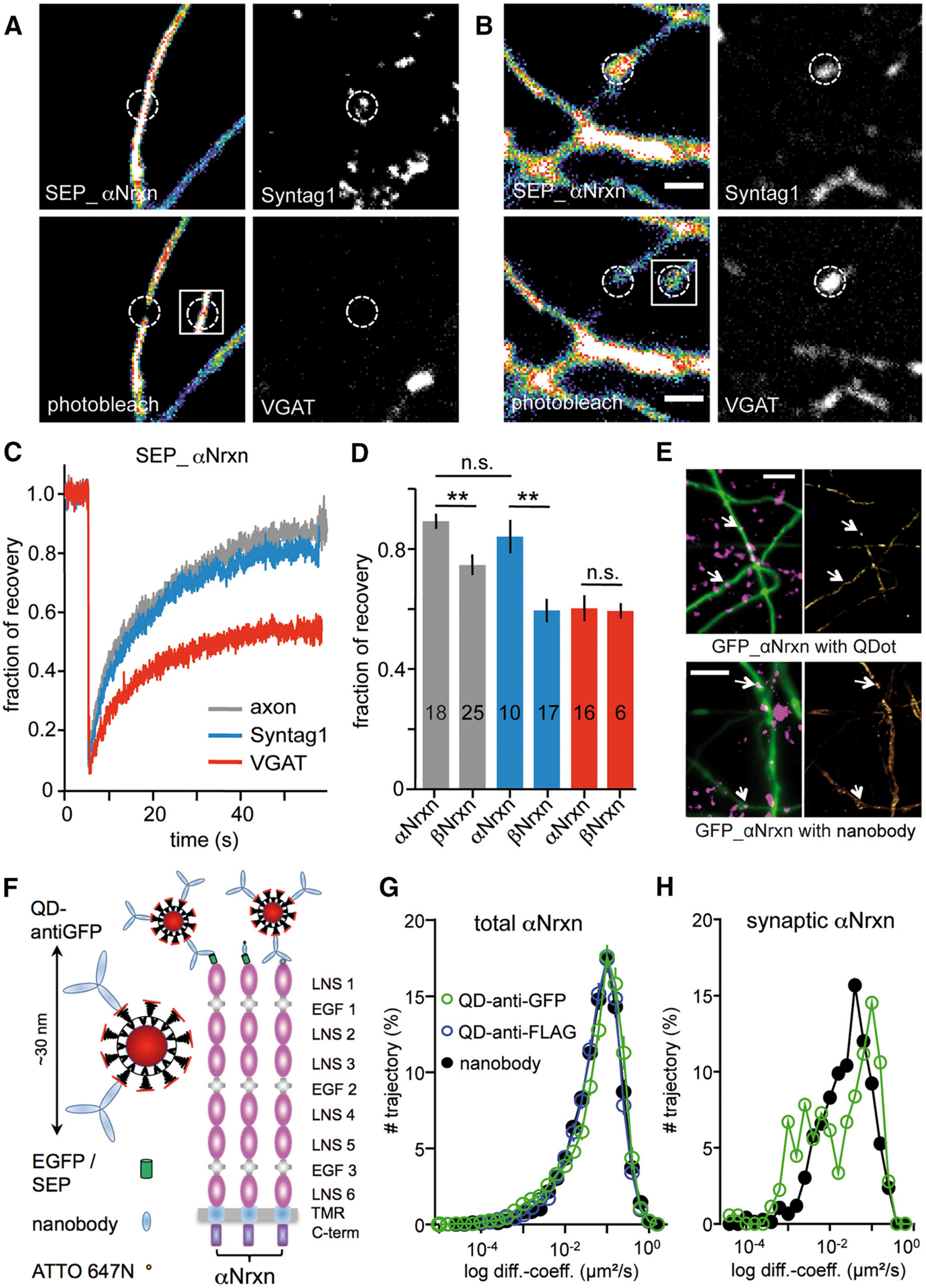

Figure 1. FRAP measurements and single-particle tracking reveal mobile epitope-tagged Nrxn molecules at the cell surface of primary rat hippocampal neurons. ***A***, Example of pHluorin(SEP)-Nrxn1α FRAP (circles indicate FRAP region, boxes show recovery after 60 s). This sample shows a putatively excitatory synapse identified by anti-synaptotagmin1 (Syntag1), but not anti-VGAT uptake. ***B***, Example for Nrxn1α FRAP at a Syntag1^{-} and VGAT^{+} putatively inhibitory terminal. Scale bars, 3 μm. ***C***, Recovery curves of αNrxn fluorescence corrected for steady-state photobleach during acquisition normalized to control fluorescent levels. Gray trace represents an extrasynaptic axonal region, blue a Syntag1^{+} region, and red a Syntag1/VGAT^{+} region. ***D***, Quantification of FRAP after 60 s for transfected SEP_Nrxn1α and SEP_Nrxn1β at axons (gray bars) and at excitatory (blue) or inhibitory (red) synapses. Data are means $\pm$ SEM collected from 6–25 synapses/FRAP regions from 3–6 cells of 3 independent cultures. Differences were tested by a one-way ANOVA followed by Newman–Keuls test. $^{**}p < 0.01$. ***E***, Sample images of axonal segments transfected with GFP_αNrxn (green) and synapses identified by Syntag1-uptake (magenta). Arrows indicate synaptic contacts. Analysis of the localization of QD- (top) or nanobody-ATTO647N (bottom)-labeled αNrxns reveals only a slight accumulation of molecules in synapses. Scale bars, 5 μm. ***F–H***, Single-particle tracking of exogenous αNrxns performed with QD or nanobodies after transfection of neurons with EGFP/SEP- or Flag-tagged Nrxn1α. Sizes in the legend of the diagram (left) are approximately to scale. ***F***, Logarithmic distribution of the surface diffusion coefficient of total αNrxn (***G***) and of synaptically localized αNrxn (***H***) tracked by QD-coupled antibodies against GFP or Flag epitopes and by nanobodies against GFP. Data were collected from 6 cells of 3 independent cultures.

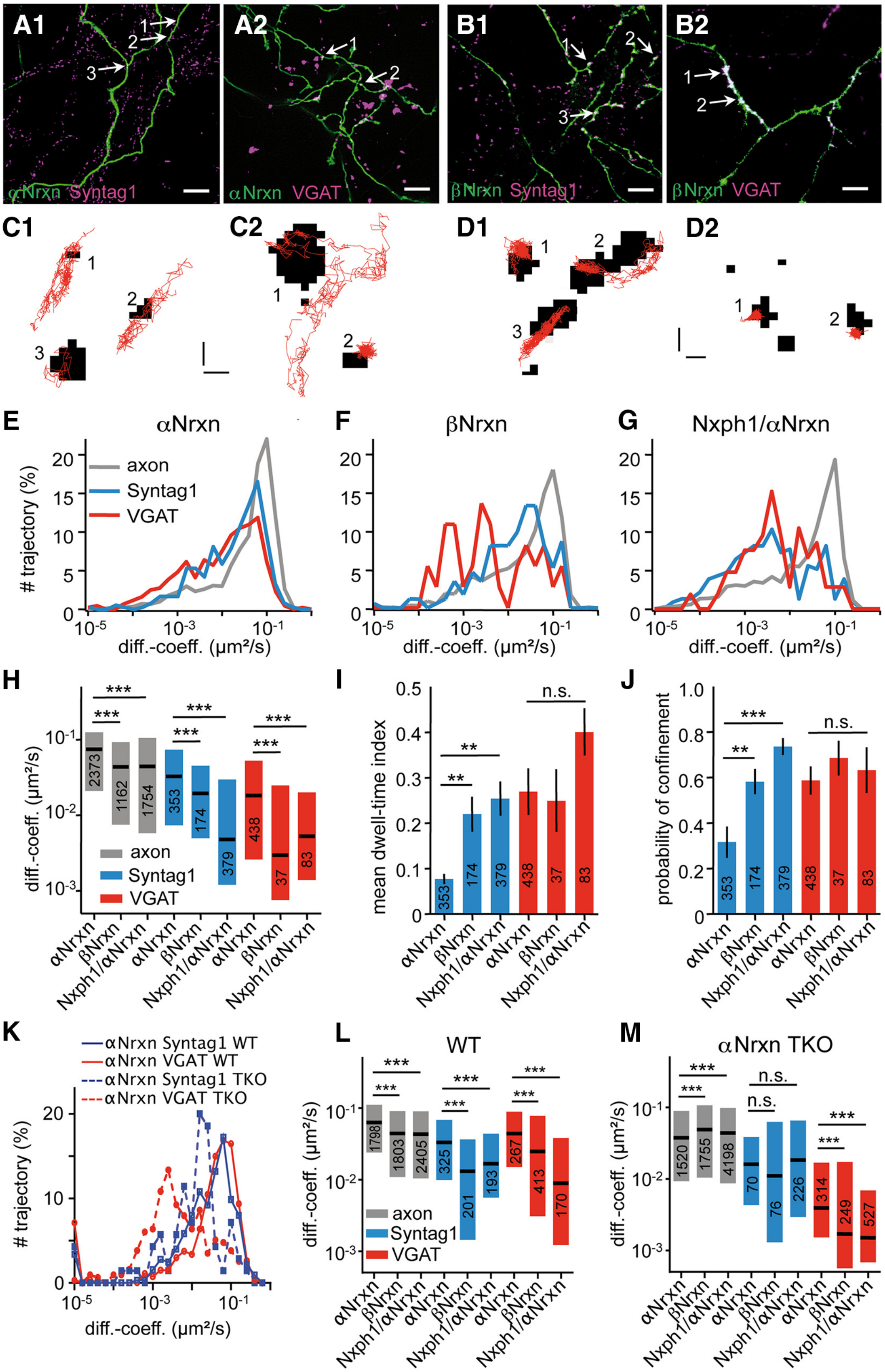

Figure 2. αNrxns and βNrxns diffuse with distinct surface mobilities extrasynaptically and within excitatory or inhibitory synapses. ***A***, ***B***, Colabeling of Nrxn1α (***A***) or Nrxn1β (***B***) surface populations on transfected rat hippocampal neurons with anti-Syntag1 and anti-VGAT to identify glutamatergic and GABAergic axons and synapses. Scale bars, 10 µm. ***C***, ***D***, Sample trajectories of QD-tracked single αNrxn (***C***) and βNrxn (***D***) molecules at positions indicated by arrows in (***A***, ***B***). Logarithmic distribution of diffusion coefficients for αNrxn (***E***), βNrxn (***F***), and cotransfected Nxph1/αNrxn complex (***G***) on axons outside synapses (black), inside excitatory (blue), and inside inhibitory (red) synapses. ***H***, Median and IQR (25–75%) of diffusion coefficients with total numbers of analyzed trajectories indicated in bars. Statistical significance was tested by Kruskal–Wallis test followed by a Dunn's test. ***I***, ***J***, Dwell-time index (***I***) and probability of confinement (***J***) of αNrxns, βNrxns, and the Nxph1/αNrxn complex reveal higher affinity of αNrxns and Nxph1/αNrxn to inhibitory terminals (red) compared with excitatory presynapses (*Figure legend continues.*)

calculated using custom software (Sergé et al., 2002). For QDs in transit between synapses, the dwell-time index was calculated as follows: time spent in synapses/(total acquisition time × number of exits). For molecules that did not leave a cluster, the dwell-time index was set to 1. Tracking of single molecules and diffusion analysis for nanobody-labeled Nrxns was done with analysis software running as plug-in for MetaMorph. Localization of single molecules used a wavelet-based identification, followed by a Gaussian fit of its fluorescence in the x and y directions. The detailed workflow and algorithms were described recently (Kechkar et al., 2013). The diffusion coefficients were analyzed similar to the QD-labeled probes using the first four points of the MSD based on trajectories longer than eight points.

Statistical analysis. Data presented are means ± SEM or represent median and interquartile range (25–75%), as indicated. Statistical significance was tested with a two-tailed unpaired Student's t test or one-way ANOVA variance test using Prism version 6.0 software (GraphPad Software). Results were denoted statistically significant at $p < 0.05$; number (n) of samples/repeats, and exact p values and significance levels are indicated in the Results and in the figure legends.

Results

Surface mobilities of fluorescently tagged αNrxns and βNrxns are distinct and specific

To visualize Nrxn at the cell surface, we transfected rat hippocampal neurons with pHluorin-tagged Nrxn1α (SEP_αNrxn) and Nrxn1β (SEP_βNrxn). We first performed FRAP in combination with labeling of active synapses using spontaneous uptake of antibodies against the luminal domains of synaptotagmin (Syntag1; Fig. 1*A*) and vesicular GABA transporter (VGAT; Fig. 1*B*; Kraszewski et al., 1995; Martens et al., 2008). This distinguished between extrasynaptic axonal sites (Syntag1$^-$ and VGAT$^-$) and excitatory (Syntag1$^+$) and inhibitory (VGAT$^+$ and Syntag1$^+$) terminals. We observed that αNrxn fluorescence recovered fully at glutamatergic, but not at GABAergic contacts, whereas βNrxn recovered only partially in both types (Fig. 1*C*,*D*). These results indicate that surface mobilities of αNrxns and βNrxns are distinct, with higher average dynamics for αNrxn (Fig. 1*D*). However, population measurements such as FRAP are limited by averaging heterogeneous molecule mobility within the area of photobleach (>1 μm). We therefore used SPT to resolve the heterogeneity (Triller and Choquet, 2008) and to investigate mobility of Nrxn molecules inside small synapses. To monitor individual pHluorin- or GFP-tagged molecules on the surface of cultured neurons, we first performed proof-of-principle experiments showing that this method is suitable for Nrxn (Fig. 1*E*–*H*). We transfected and overexpressed Nrxn1α fused to tags of different sizes (EGFP and Flag) and tested larger QD-coupled antibodies or smaller nanobodies (Fig. 1*E*,*F*). The diagram in Figure 1*F* shows an approximate comparison of the sizes for different labels used. These recordings resulted in virtually identical diffusion coefficients on axons (D ≈ 0.07 μm^2/s; Fig. 1*G*). Within synaptic terminals, nanobodies demonstrated a more homogeneous distribution of Nrxn1α diffusion, whereas QD tracking also revealed an additional, more immobile population (Fig. 1*H*). Importantly, however, QD and nanobodies both determined the diffusion of mobile Nrxn molecules in synapses at very similar values (Fig. 1*H*), indicating that the surface diffusion coefficient of mobile αNrxn is amazingly independent of the nature of the tag and tracking system. We therefore opted to use the well characterized QD-coupled anti-GFP antibodies for most SPT experiments because this label allows us, not only to explore diffusion reliably, but also to determine the relative dwell time and confinement area in different membrane compartments (Groc et al., 2007; Heine et al., 2008a; Di Biase et al., 2011; Mondin et al., 2011; Biermann et al., 2014).

Single-molecule mobilities of αNrxn and βNrxn differ on neurites and within synapses

To evaluate surface mobility in different compartments, we combined QD tracking of αNrxn and βNrxn molecules with live labeling of excitatory and inhibitory synaptic terminals (Fig. 2*A*,*B*), as described above for FRAP (Fig. 1). Trajectories of QD tracks (Fig. 2*C*,*D*) or distribution of diffusion coefficients (Fig. 2*E*,*F*) demonstrated that most Nrxn molecules, in particular αNrxn, belong to a very mobile population ($D > 10^{-3}$ μm^2/s) that is only transiently confined at synapses. We found that, at extrasynaptic sites on axons, αNrxn molecules are more mobile than βNrxn molecules (Fig. 2*H*). Diffusion coefficients showed that αNrxn molecules are almost twice as mobile [αNrxn: median 0.071 μm^2/s, interquartile range (IQR) = 0.019/0.12, n = 2608 trajectories; βNrxn: 0.044, IQR = 0.0075/0.093, n = 1162 trajectories], a surprising observation given the much longer extracellular sequences. These experiments further revealed that αNrxns have higher diffusion rates inside excitatory and inhibitory synapses compared with βNrxns (Fig. 2*H*). This difference was reflected by a lower dwell time index and reduced synaptic confinement, at least in excitatory terminals (Fig. 2*I*,*J*). We then compared the mobility of axonal Nrxn with their diffusion on dendrites because the presence of a small postsynaptic population was proposed (Kattenstroth et al., 2004; Taniguchi et al., 2007). On dendrites, αNrxns showed also higher mobility than βNrxns, but with a >10-fold difference, even though much fewer trajectories were visible on dendrites in general (αNrxn: median: 0.012, IQR = 0.002/0.036, n = 483 trajectories; βNrxn: 0.0006, IQR = 0.0002/0.0011, n = 88 trajectories). Together, our SPT data reveal that Nrxn have an unexpectedly high surface mobility for a so-called synaptic cell adhesion molecule and that αNrxns, despite their larger extracellular domain, are more mobile than βNrxns, even inside terminals.

To determine whether the high surface mobility is simply a consequence of overexpressing tagged Nrxn in addition to endogenous Nrxn molecules, we performed SPT experiments in neurons from triple knock-out (TKO) mice that lack all αNrxn (Missler et al., 2003). A comparison of the dynamics of αNrxn and βNrxn in neurons from rats (Fig. 2*H*) and wild-type (WT) mice (Fig. 2*L*) revealed that their surface mobilities were similar, showing the same significantly higher mobility of αNrxns. These data exclude prominent species-specific differences and confirm the distinct mobilities measured in FRAP experiments of primary neurons from rat (Fig. 1*A*–*D*) and of slice cultures from mice (Fu and Huang, 2010). Interestingly, the frequency distribution of diffusion coefficients for αNrxns analyzed within synaptic terminals of TKO neurons showed a shift to lower mobilities compared with WT (Fig. 2*K*). Because βNrxn mobility was largely unchanged on axons or in excitatory synapses of αNrxn-deficient TKO neurons, the average diffusion of αNrxns was even lower than βNrxns at extrasynaptic sites and indistinguishable in excit-

←

(*Figure legend continued.*) (blue). Numbers in bars (***H***–***J***) represent analyzed Nrxn$^+$ synapses from 3–10 rat neuronal cultures and 4–27 cells. Data in ***I*** and ***J*** are expressed as means ± SEM and statistical significance was assessed by one-way ANOVA variance followed by Newman–Keuls test. $^{**}p < 0.001$, $^{***}p < 0.0001$. ***K***–***M***, Comparison of surface mobility in hippocampal neurons from WT mice and TKOs lacking endogenous αNrxns. Diffusion coefficients for αNrxns in excitatory (blue) and inhibitory (red) terminals of WT (solid line) and TKO (dashed) neurons (***K***). Surface mobility was analyzed in transfected WT (***L***) and TKO (***M***) mouse neurons as in ***H***. Numbers in bars (***L***, ***M***) represent the total number of analyzed trajectories from 2–3 mouse hippocampal cultures with 5–17 neurons per genotype.

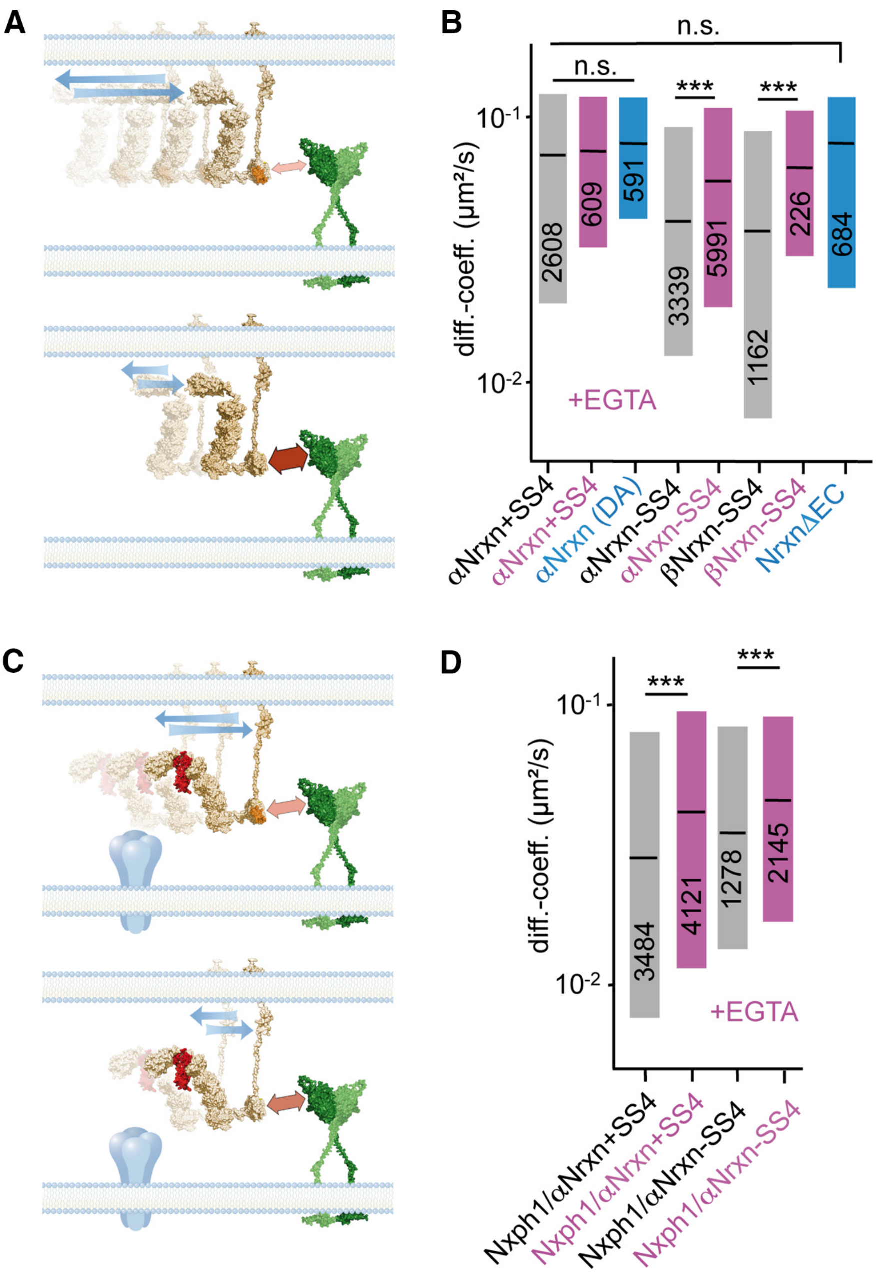

Figure 3. Surface mobility of Nrxns depends on alternative splicing and extracellular Ca^{2+} concentration. ***A***, ***B***, Comparison of mobility between Nrxn1α without insert in SS4 (beige in scheme ***A***, −SS4 in ***B***) and with insert (SS4 orange in scheme ***A***, +SS4 in ***B***) and of Nrxn1$\beta \pm$SS4, measured by SPT. Extracellular domains are replaced by EGFP to have a reference for maximal diffusion dynamics (NrxnΔEC). Chelation of extracellular calcium with 10 mM EGTA (magenta) is used to assess the general effect of Ca^{2+}-dependent binding activities, for example, with postsynaptic Nlgn (green in schemes). Ca^{2+} coordination of the LNS6 domain alone is impaired in the point mutation D1183A (αNrxn (DA; Reissner et al., 2008). ***C***, ***D***, Similar experiment as in ***A*** and ***B***, but probing the effect of complex formation of αNrxn $\pm$ SS4 with cotransfected Nxph1 (red in schemes) on surface mobility. In ***B*** and ***D***, the median and IQR (25–75%) of diffusion coefficients with total numbers of analyzed trajectories are indicated in bars. Statistical significance was tested by Kruskal–Wallis test followed by a Dunn's test. ***$p < 0.0001$.

atory synapses (Fig. 2*M*). In contrast, αNrxns and βNrxns both displayed lower mobilities inside the inhibitory synapses of αNrxn TKO (Fig. 2*M*), thereby maintaining the difference observed in WT (Fig. 2*H*,*L*). These data indicate that overexpression of fluorescently tagged αNrxns in WT neurons leads to a moderate overestimation of their average surface mobility. Future experiments in βNrxn KO mice will have to test whether the absolute mobility of βNrxns was also slightly overestimated in WT neurons, likely reinstating the difference between αNrxns and βNrxns in front of their respective null backgrounds. More importantly, however, we conclude that removal of endogenous protein did not abolish the mobility of αNrxns, a remarkable finding for a molecule capable of multiple *trans*-synaptic interactions (Reissner et al., 2013). In addition, the TKO background did not change characteristic differences between αNrxn mobilities at extrasynaptic sites and inside both types of terminals (Fig. 2*M*), suggesting that the much lower diffusion in inhibitory terminals is an important property. Finally, the difference between αNrxns and βNrxns in WT neurons (Fig. 2*H*,*L*), which disappeared in αNrxn TKO neurons, is largely due to lower αNrxn diffusion with unchanged βNrxn diffusion (Fig. 2*M*). These data argue for a specificity of their respective surface mobilities, supporting our previous hypothesis of mostly nonredundant functions of αNrxns and βNrxns (Zhang et al., 2005). Together, our results suggest that SPT of tagged Nrxns reliably reflects their distinct dynamics inside and outside of synapses.

Surface mobilities of Nrxns are regulated by extracellular binding activities

An explanation for the higher mobility of Nrxn1α compared with Nrxn1β, which share identical C-terminal sequences, may consist of specific binding activities of their distinct extracellular domains. To investigate this idea, we first made use of the αNrxn-specific binding partner Nxph1 (Missler and Südhof, 1998). In contrast to Nrxn, Nxph isoforms are restricted to subpopulations of neurons (Petrenko et al., 1996; Beglopoulos et al., 2005), presenting a test case if local availability of interaction partners alters diffusion dynamics. Strikingly, coexpression of Nxph1 strongly reduced the mobility of αNrxns within synapses of rat and mouse WT neurons (Fig. 2*G*,*H*,*L*). The diffusion coefficient of the Nxph1/αNrxn complex within excitatory ($D = 0.0048\ \mu m^2/s$) and inhibitory ($D = 0.0052\ \mu m^2/s$) terminals dropped compared with αNrxn alone ($D_{exc} = 0.033\ \mu m^2/s$, $D_{inh} = 0.018\ \mu m^2/s$; Fig. 2*H*,*L*), and this was accompanied by an increase of the dwell time and confinement in glutamatergic but not inhibitory synapses (Fig. 2*I*,*J*). In αNrxn TKO neurons, the Nxph1/αNrxn complex mobility was not reduced extrasynaptically and at excitatory terminals compared with αNrxns alone, whereas dynamics were still lower in inhibitory synapses (Fig. 2*M*). These results could indicate that coexpression of Nxph1 with αNrxns encounters additional binding partners in GABAergic terminals, leading to reduced mobility independent of the presence of endogenous αNrxns. This is a physiologically attractive hypothesis because we recently showed that genetic deletion or transgenic overexpression of Nxph1 in mice actually modulates inhibitory synaptic function and receptors (Born et al., 2014).

To extend our analysis to the influence of *trans*-synaptic binding activities and to include βNrxn in this analysis, we next examined the role of alternative splicing at splice site 4 (SS4) and of Ca^{2+} sensitivity in Nrxn surface mobility (Fig. 3*A*). These parameters are crucial because they determine interactions of Nrxn with postsynaptic partners neuroligins, LRRTMs, cerebellin, and dystroglycan (Ichtchenko et al., 1995; Sugita et al., 2001; Boucard et al., 2005; Reissner et al., 2008; Ko et al., 2009; de Wit et al., 2009b; Uemura et al., 2010; Matsuda and Yuzaki, 2011). If the relative immobility of βNrxn depends on stronger binding to these partners, we should see a higher mobility in the absence of Ca^{2+} or with splice variants carrying an insert in SS4. Extracellular chelation of Ca^{2+} by 10 mM EGTA in fact mobilized βNrxns, but did not alter the diffusion of an extracellularly truncated version of Nrxn used as a control (NrxnΔEC; Fairless et al., 2008; Fig. 3*B*). We also tested the Ca^{2+}-dependent mobility of the splice variants αNrxn(−SS4) and αNrxn(+SS4), which differ in their Ca^{2+}-dependent binding affinities to neuroligin-1 because presence of the splice insert impedes the interaction (Reissner et al., 2008). In agreement, the mobility of the αNrxn(+SS4) variant did not show changes to extracellular Ca^{2+} chelation or mutation of its Ca^{2+} interaction site [αNrxn(DA); Fig. 3*B*], whereas αNrxn(−SS4) was more mobile at a low

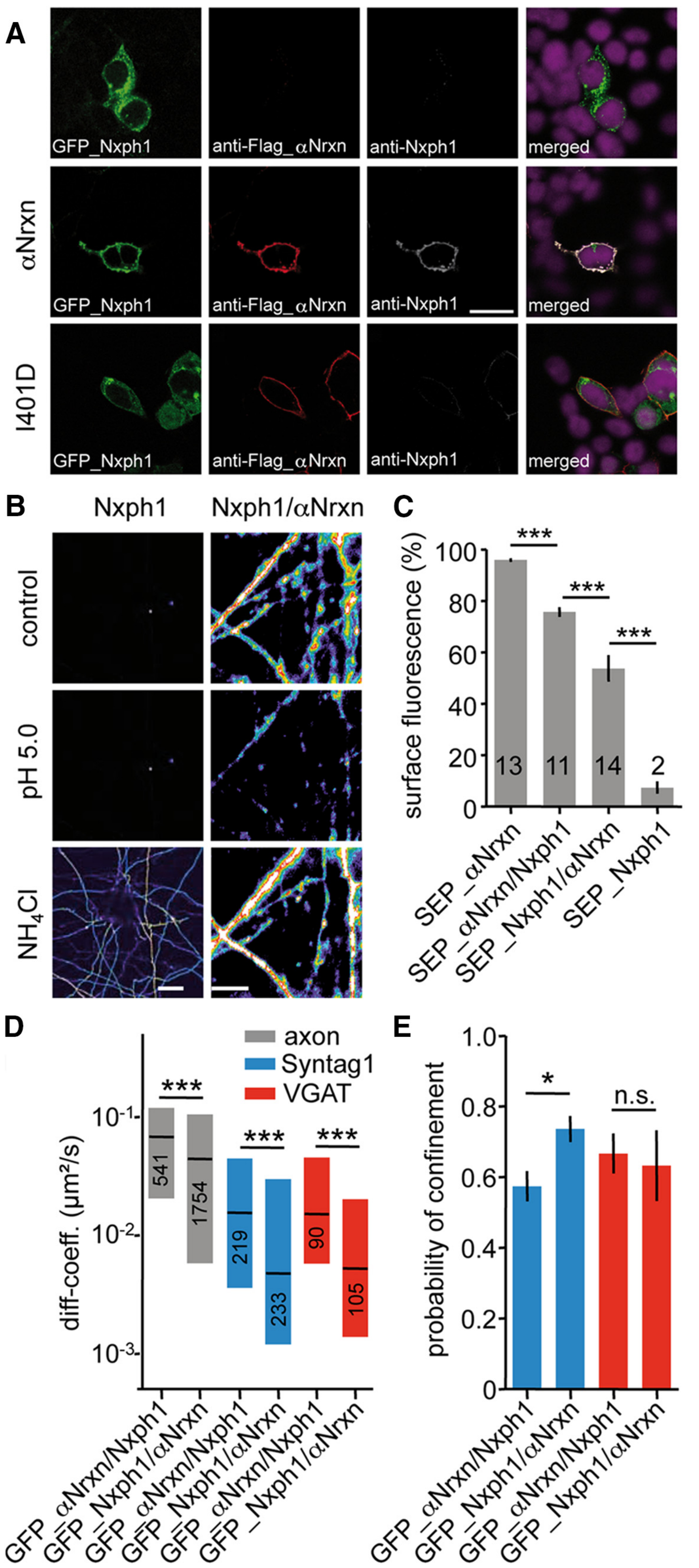

Figure 4. Nxph1 requires coexpression with αNrxns for targeting but not vice versa. ***A***, GFP-tagged Nxph1, when transfected alone, accumulates inside heterologous HEK293 cells and is not detected extracellularly at the cell surface by live labeling with antibodies against Nxph1 (top). Cotransfection of GFP-Nxph1 with a Flag-tagged full-length Nrxn1α results in a ring-like staining pattern of colocalized Nxph1/αNrxn by live labeling with antibodies to the Flag_Nrxn1α and Nxph1 moieties (middle panels).

←

Mutation of a key binding residue in αNrxn (I401D; Reissner et al., 2014) prevents surface delivery of Nxph1 (bottom). Scale bar, 20 µm. ***B***, Sample images of pHluorin(SEP)_Nxph1 (left; scale bar, 20 µm) and SEP_Nxph1/αNrxn (right; scale bar, 5 µm) cotransfected into primary neurons under control buffer conditions at pH 5.0 and after NH$_4$Cl treatment to equilibrate intracellular and extracellular pH at 7.4. ***C***, Nxph1 coexpressed with αNrxns is detected at the cell surface independently of which moiety carries the pHluorin. Quantification of surface fluorescence within axons in (%) of the total fluorescence is shown. Data are means ± SEM collected from 2–14 cells of 2–3 hippocampal cultures at DIV 14–21. ***D***, ***E***, Complex formation with Nxph1 decreases the surface mobility of αNrxns at synapses. Median and IQR (25–75%) of diffusion coefficients (***D***) and probability of confinement (***E***) of cotransfected Nxph1/αNrxn complexes are shown, in which either αNrxns or Nxph1 carried the EGFP tag. Total numbers of analyzed trajectories are indicated in bars. Statistical significance in ***C–E*** is tested by Kruskal–Wallis test followed by a Dunn's test. $*p < 0.05$, $***p < 0.0001$.

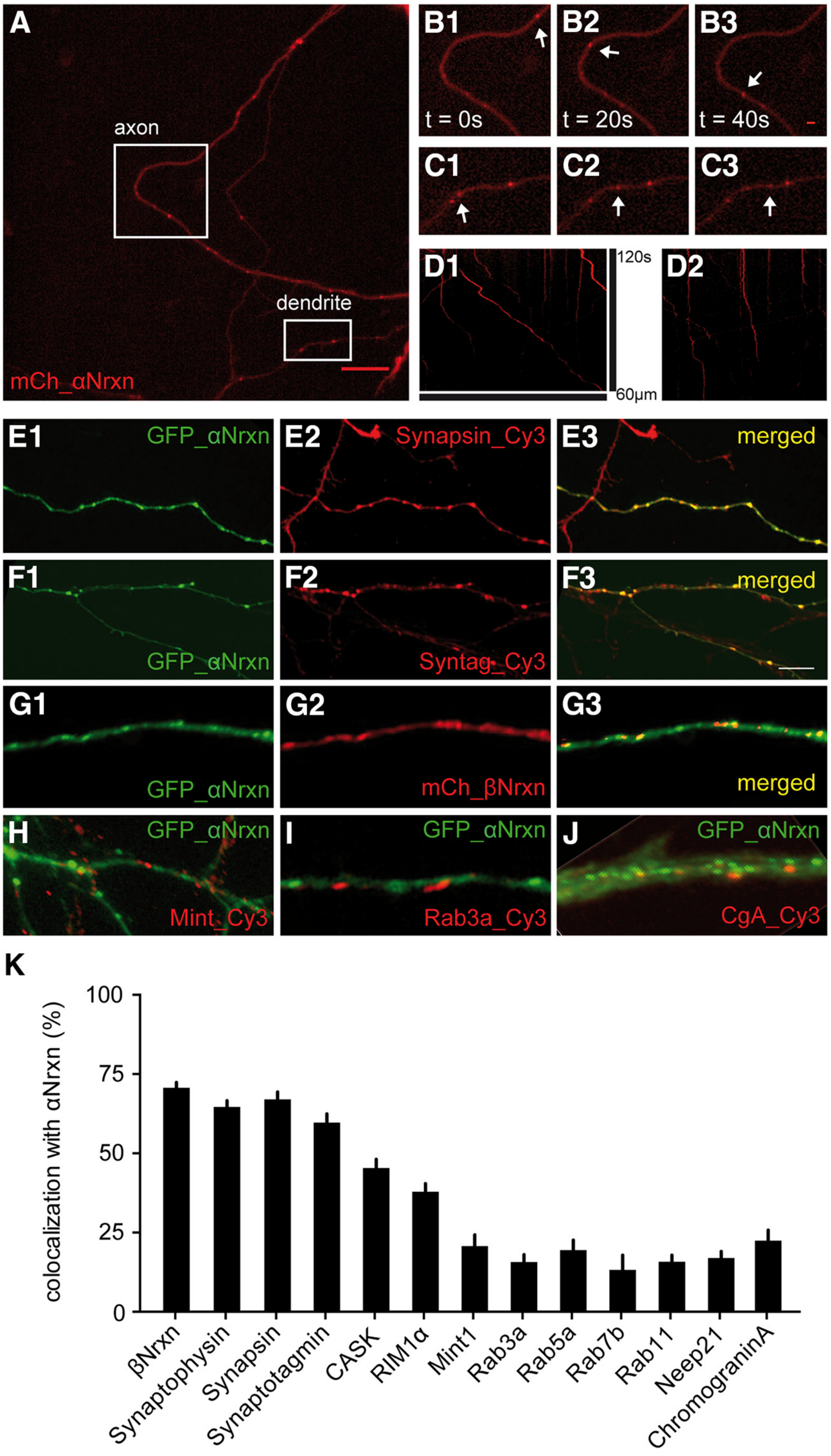

Figure 5. Intracellular Nrxn$^+$ transport vesicles colocalize with marker molecules of STVs. ***A–D***, Examples of Nrxn1α$^+$ transport vesicles migrating within axons (***B***, marked area in ***A***) and dendrites (***C***, marked area in ***A***) in primary hippocampal neurons. Their velocity was determined from respective kymographs as in ***D***. Scale bars: ***A***, 20 μm; ***B***, ***C***, 5 μm. ***E–J***, GFP_αNrxn$^+$ transport vesicles colocalized strongly with STV marker proteins as synapsin (***E***) and synaptotagmin1 (***F***) and also with Nrxn1β (***G***). Double labeling of GFP_αNrxn with Mint1 (***H***), the synaptic vesicle precursor Rab3a, and chromogranin-A as a DCV component (***J***) was less apparent. Scale bar in ***F3***, 10 μm. ***K***, Degree of colocalization was expressed as percentage overlap with GFP_αNrxn using ImageJ. Data are expressed as means ± SEM and were derived from a total of 671 neurons/38 transfected cultures.

Ca^{2+} concentration (Fig. 3*B*). Importantly, coexpression of Nxph1 with αNrxn(+SS4) or αNrxn(−SS4) strongly increased the Ca^{2+} sensitivity for both variants (Fig. 3*C*,*D*). Although our experiments with Ca^{2+} chelation or alternative splicing did not allow us to determine directly which postsynaptic partners contribute to the effect, recent biochemical data allow a hypothesis: the enhanced sensitivity of the Nxph1/αNrxn complex to Ca^{2+}-dependent binding activities could suggest that the Nxph1 association with the LNS2 domain of αNrxn blocks the interaction with α-dystroglycan at the same LNS2 domain (Reissner et al., 2014). Such a scenario should be particularly prominent for the most abundant splice variant in cortical neurons, αNrxn(+SS4) (Ullrich et al., 1995; Aoto et al., 2013), which favors association with neuroligins lacking the B insert (Reissner et al., 2014) and consistently showed a large increase in surface mobility when Ca^{2+} was chelated (Fig. 3*D*).

Surface targeting and mobility of Nxph1 requires αNrxn

The strong effect of Nxph1 on αNrxn diffusion raised the question of whether Nxph1 is only active when bound to αNrxn. Based on our analysis of the binding epitope (Reissner et al., 2014), we hypothesized that correct folding of Nxph1 and formation of the Nxph1/αNrxn complex requires coexpression in the same cell. Here, we addressed this idea directly by transfecting GFP_Nxph1 alone and in combination with Flag_Nrxn1α into heterologous cells that contain neither molecule endogenously (Fig. 4*A*). We discovered that efficient targeting of Nxph1 to the surface required coexpression with αNrxn and that, in transfections of Nxph1 alone, no surface population could be detected by live incubation with antibodies against Nxph1 (Fig. 4*A*). Moreover, cotransfection of Nxph1 with an αNrxn carrying a single point mutation that strongly reduces binding (I401D; Reissner et al., 2014) showed only very little Nxph1 at the surface (Fig. 4*A*). These data indicate that normal complex formation with αNrxn is necessary and sufficient to deliver Nxph1 to the surface, at least in heterologous cells.

We next validated the strong dependence of Nxph1 on αNrxns in neurons. The pHluorin-tagged constructs failed to detect significant surface populations of Nxph1 when it was transfected alone (Fig. 4*B*,*C*). Coexpressed Nxph1/αNrxn, in contrast, was reliably observed at the neuronal surface independently of which partner carried the pHluorin moiety (Fig. 4*B*,*C*). Interestingly, a proportion of the pHluorin_Nxph1/αNrxn complex remained intracellularly, as evident from the lower surface expression compared with pHluorin_αNrxn alone (Fig. 4*C*). Coexpression of a pHluorin_αNrxn/Nxph1 complex,

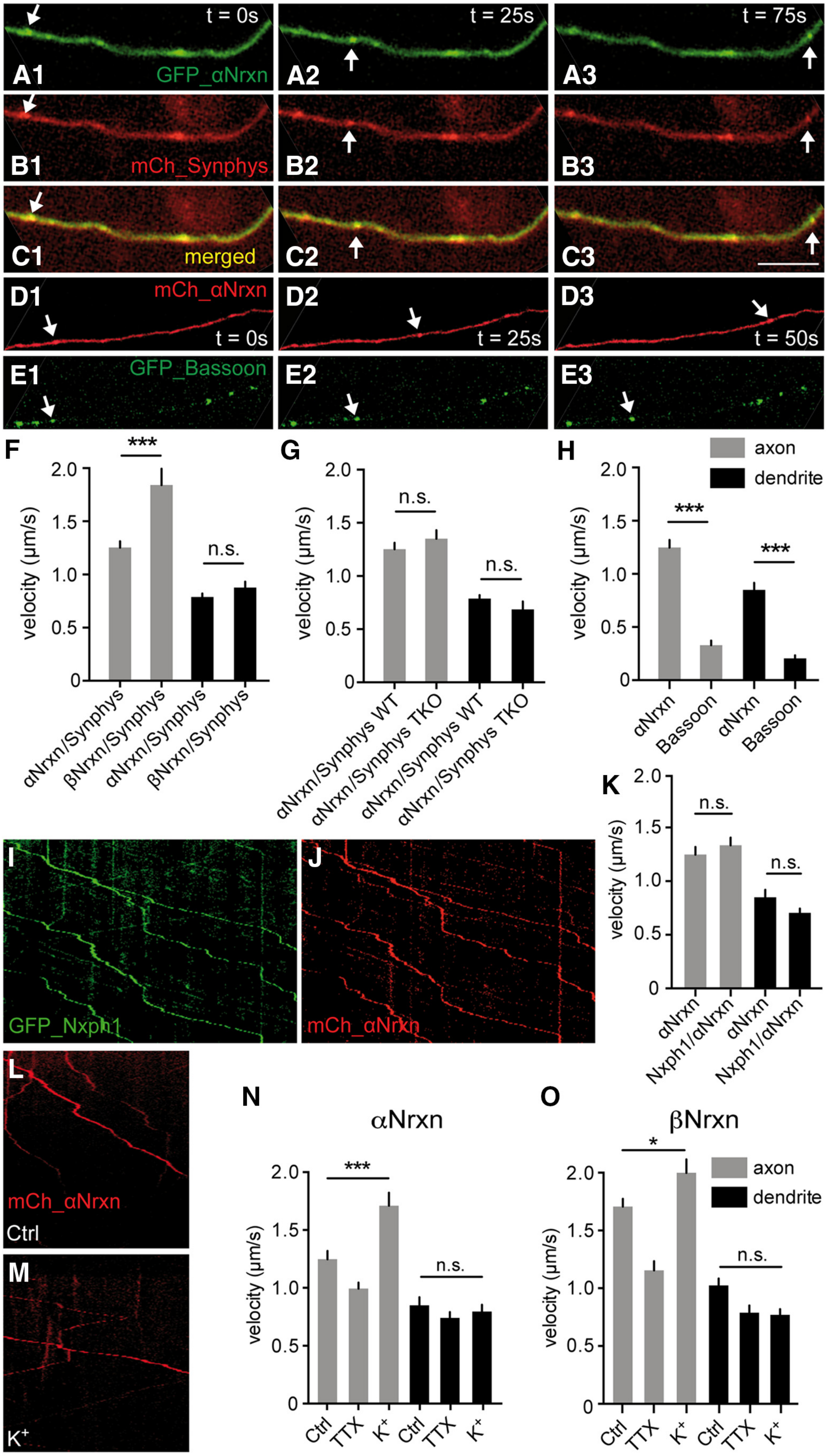

Figure 6. Distinct velocities and regulation of αNrxn- and βNrxn$^+$ STVs. ***A–C***, Example of GFP_Nrxn1α comigrating with mCherry_synaptophysin at the speed of fast axonal transport in axons of primary hippocampal neurons. ***D***, ***E***, No comigration and different speed was observed with cotransfected bassoon as marker protein of PTVs. Scale (*Figure legend continues.*)

in which αNrxn carried the fluorochrome, displayed an intermediate surface fluorescence (Fig. 4*C*). We therefore hypothesized that not all αNrxn molecules were complexed to Nxph1, even when coexpressed in the same cell. We tested this idea by comparing the surface mobility of the two coexpression versions of the complex, pHluorin/GFP_Nxph1/αNrxn or pHluorin/GFP_αNrxn/Nxph1, using QD-coupled anti-GFP for SPT. We observed that the diffusion coefficient was always lower when Nxph1 carried the tracked pHluorin/GFP moiety (Fig. 4*D*). This result indicates that a proportion of uncomplexed αNrxn molecules reached the surface when pHluorin/GFP_αNrxn and Nxph1 were cotransfected. This effect was particularly prominent inside synaptic terminals compared with extrasynaptic sites (Fig. 4*D*) without increasing confinement strongly (Fig. 4*E*). Together, these findings indicate that neurons restrict the amount of more immobile Nxph1/αNrxn complexes at their surface compared with αNrxns alone. Such a restriction raises the question, however, of if and how delivery from intracellular pools contributes to the surface population of Nrxn.

STVs transport Nrxn toward synapses

To analyze how Nrxns and the Nxph1/αNrxn complex are targeted to the surface and to synapses, we built on an earlier study in which we revealed that Nrxns require their C-terminal PDZ-recognition motif to traverse the secretory pathway via a hitherto uncharacterized class of transport vesicles (Fairless et al., 2008). Although this earlier study relied on immunolabeling of fixed neuronal cultures, we now used live imaging to characterize the dynamic trafficking of Nrxns. We first transfected primary hippocampal neurons separately with GFP- or mCherry-tagged αNrxns and βNrxns and then studied the migration of their transport vesicles in axonal and dendritic processes (Fig. 5*A–C*). We observed that Nrxn$^+$ vesicles primarily show a unidirectional, anterograde movement in axons, whereas they moved more bidirectionally in dendrites. This was quantitatively reflected by a tendency, albeit not significant, for more pausing vesicles (axon: 0.013 ± 0.001 pauses/s, dendrite: 0.017 ± 0.003; $p = 0.18$), which is consistent with published data (Sabo et al., 2006; Bury and Sabo, 2011). To determine the velocity of mobile Nrxn$^+$ transport vesicles, we analyzed their kymographs (Fig. 5*D*). Strikingly, we found that Nrxns generally move faster within axons (Nrxn$_{\mathrm{ax}}$) than in dendrites (Nrxn$_{\mathrm{de}}$) and that αNrxns migrate more slowly than βNrxns (αNrxn$_{\mathrm{ax}}$: 1.2 ± 0.071 μm/s, αNrxn$_{\mathrm{de}}$: 0.8 ± 0.070, $p = 0.0091$; βNrxn$_{\mathrm{ax}}$: 1.7 ± 0.067, βNrxn$_{\mathrm{de}}$: 1.0 ± 0.062, $p = 0.0001$; $n = 45–47$ cells/4 transfected cultures per condition). Although the values in axons are within the published range of fast vesicular transport (Vallee and Bloom, 1991) and argue for transport on STVs or DCVs, other pathways such as PTVs or endosomes cannot be excluded based on velocities alone. We therefore performed colabeling experiments with known marker proteins (Fig. 5*E–J*) and quantified colocalization by percentage of colabeled vesicles (Fig. 5*K*). αNrxns and βNrxns showed a high degree of colocalization with synaptophysin, synapsin, and synaptotagmin-1 (60–75%; Fig. 5*K*), established markers of STVs (Ahmari et al., 2000; Sabo et al., 2006). In addition, proteins directly or indirectly associated with the C terminus of Nrxn, such as CASK or Rim1α, were also frequently colocalized during trafficking (Fig. 5*K*), confirming earlier data (Fairless et al., 2008). In contrast, markers such as Rab3a for synaptic vesicle precursors, Rab5a for early endosomes, Rab7b for late endosomes/lysosomes, Rab11 or NEEP21 for recycling endosomes, and chromograninA for DCVs revealed only moderate or little colocalization (Fig. 5*K*). These data suggest that Nrxns are primarily transported as cargo on STVs, pointing to a major pathway toward synapses.

To prove that Nrxns not only colocalize with relevant markers, but actually comigrate with STVs, we cotransfected GFP-tagged αNrxn or βNrxn along with mCherry-tagged synaptophysin and observed mostly synchronous movements (Fig. 6*A–C*). As a negative control, we repeated the experiment with mCherry_αNrxn and GFP_Bassoon, a marker for PTVs that move at slower speed, and found no comigration (Fig. 6*D*,*E*). We then determined the velocity of αNrxn/synaptophysin- and βNrxn/synaptophysin-colabeled STVs from kymographs separately in axons and dendrites. Mobile Nrxn/synaptophysin$^+$ STVs were present in all processes, in agreement with our data from fixed cultures (Fairless et al., 2008), but they were generally faster in axons compared with dendrites (Fig. 6*F*), confirming our initial observation (Fig. 5). Interestingly, βNrxn$^+$ STVs moved with a higher velocity than αNrxn in axons, whereas no significant difference was found in dendrites (Fig. 6*F*). To rule out the possibility that these differences were simply caused by the presence of endogenous protein, of which there is more αNrxns than βNrxns in brains (Schreiner et al., 2015), we performed the experiment in TKO neurons lacking all αNrxns (Missler et al., 2003). However, no difference was observed between the velocity of αNrxn/synaptophysin$^+$ STVs in control and TKO neurons (Fig. 6*G*), suggesting that overexpressed Nrxns reliably reflected their intracellular trafficking. Finally, to evaluate the presence and velocity of different classes of transport vesicles in the same neuron, we cotransfected labeled αNrxns and bassoon and found higher speed for Nrxn$^+$ STVs in axons and dendrites compared with bassoon$^+$ PTVs (Fig. 6*H*), consistent with their nonoverlapping migration (Fig. 6*D*,*E*). Similar to surface mobility, these data from intracellular transport reveal distinct dynamics for αNrxns and βNrxns, but with opposite results; that is, βNrxn$^+$ STVs migrated faster than αNrxns, at least in axons.

Determinants of intracellular transport of Nrxns differ from surface diffusion

To determine whether intracellular transport of Nrxn is regulated by Nxph1 binding, as was shown for surface mobility (Figs. 2, 3, 4), we cotransfected Nxph1/αNrxn and determined the velocities from kymographs compared with uncomplexed αNrxn (Fig. 6*I*,*J*). Unlike its effect on surface mobility, complex formation of Nxph1/αNrxn did not change the velocity of STVs in axons or dendrites (Fig. 6*K*). To rule out the possibility that coexpression of Nxph1 acts by altering the preference of αNrxns for axonal targeting, we compared pHluorin-(SEP)_Nxph1 and HA_Nrxn1α fluorescence intensity normalized to cotransfected soluble RFP (Biermann et al., 2010) and found a similar axon-to-dendrite ratio [Nxph1/RFP = 2.86, Nrxn1α/RFP = 2.34, $n = 7$ cells, nonsignificant (n.s.)]. Together, these results suggest that αNrxn$^+$ STVs move with defined velocity independently of the binding of Nxph1.

←

(*Figure legend continued.*) bar, 5 μm. ***F***, Comparison of comigrating αNrxn/synaptophysin$^-$ and βNrxn/synaptophysin$^+$ STVs in axons (gray bars) and dendrites (black bars). ***G***, Comparison of αNrxn/synaptophysin mobility in control (WT) and TKO neurons lacking all endogenous αNrxn. ***H***, αNrxn$^+$ STVs migrate faster than bassoon$^+$ PTVs when cotransfected into the same neurons. ***I–K***, Coexpression of Nxph1 with αNrxn has no effect on the velocity of intracellular traffic in axons and dendrites. ***L–O***, Kymographs and average velocities of Nrxn$^+$ STVs under control conditions and after incubation with TTX or K$^+$ to modulate neuronal activity. Data in ***F–H***, ***K***, ***N***, and ***O*** are expressed as means ± SEM and were derived from a total of >220 neurons/24 transfected cultures. Statistical significance was tested by Student's *t* test. $^{***}p < 0.001$.

Because several studies indicated that neuronal activity modulates the velocity of STVs carrying other synaptic cell adhesion molecules (de Wit et al., 2006; Wittenmayer et al., 2009), we also addressed this aspect. We reduced activity with 1 μM TTX or enhanced it with high potassium stimulation (60 mM K$^+$ for 30 min before imaging). As was evident from representative kymographs (Fig. 6*L*,*M*), αNrxn$^+$ and βNrxn$^+$ STVs within axons reduced their velocity under TTX, but increased migration with stimulation (Fig. 6*N*,*O*). In contrast, we observed no alterations of the velocity of Nrxn$^+$ STVs in dendrites under identical conditions (Fig. 6*N*,*O*), suggesting that the axonal, but not dendritic, population of Nrxn$^+$ STVs is regulated by changes in neuronal activity. Interestingly, the difference in axonal velocity between αNrxns and βNrxns disappeared under reduced activity and became much less apparent with enhanced activity (Fig. 6*N*,*O*), revealing that Nrxns are cargo on the same type of STVs, as suspected from their colocalization (Fig. 5*G*).

Finally, to determine whether intracellular transport of Nrxn depends on the microtubule cytoskeleton and on the motor protein KIF1A, as predicted for STVs (Hirokawa et al., 2009), we performed pharmacological experiments that interrupt different cytoskeletal elements. We treated transfected cultures with 5 μM nocodazol to inhibit microtubule polymerization or with 2.5 μM latrunculin-A to block F-actin formation (de Wit et al., 2006; Wittenmayer et al., 2009). We observed breakdown of the actin cytoskeleton with fluorochrome-coupled phalloidin and of the microtubule integrity with anti-tubulin antibodies (data not shown). We then compared the effect on Nrxn-STV migration (Fig. 7*A*,*B*) and found that Nrxn$^+$ STVs moved with normal velocity under control conditions and latrunculin-A (e.g., αNrxn in axons with DMSO: 1.31 ± 0.08 μm/s; with latrunculin-A: 1.36 ± 0.14, $n = 53$ neurons/4 transfections, n.s.). Under nocodazol, however, Nrxn$^+$ vesicles remained relatively immobile, showing little movement in axons or dendrites (αNrxn in axons with nocodazol: 0.24 ± 0.02 μm/s, $p < 0.001$). To support these data, we investigated whether KIF1A is the molecular motor involved in transporting Nrxn$^+$ STVs. We determined a high degree of colocalization and comigration of Nrxn with transfected GFP_KIF1A (Fig. 7*C*–*F*), but also with endogenous KIF1A visualized by immunolabeling (Fig. 7*G*). The velocities of αNrxn/KIF1A$^+$ and

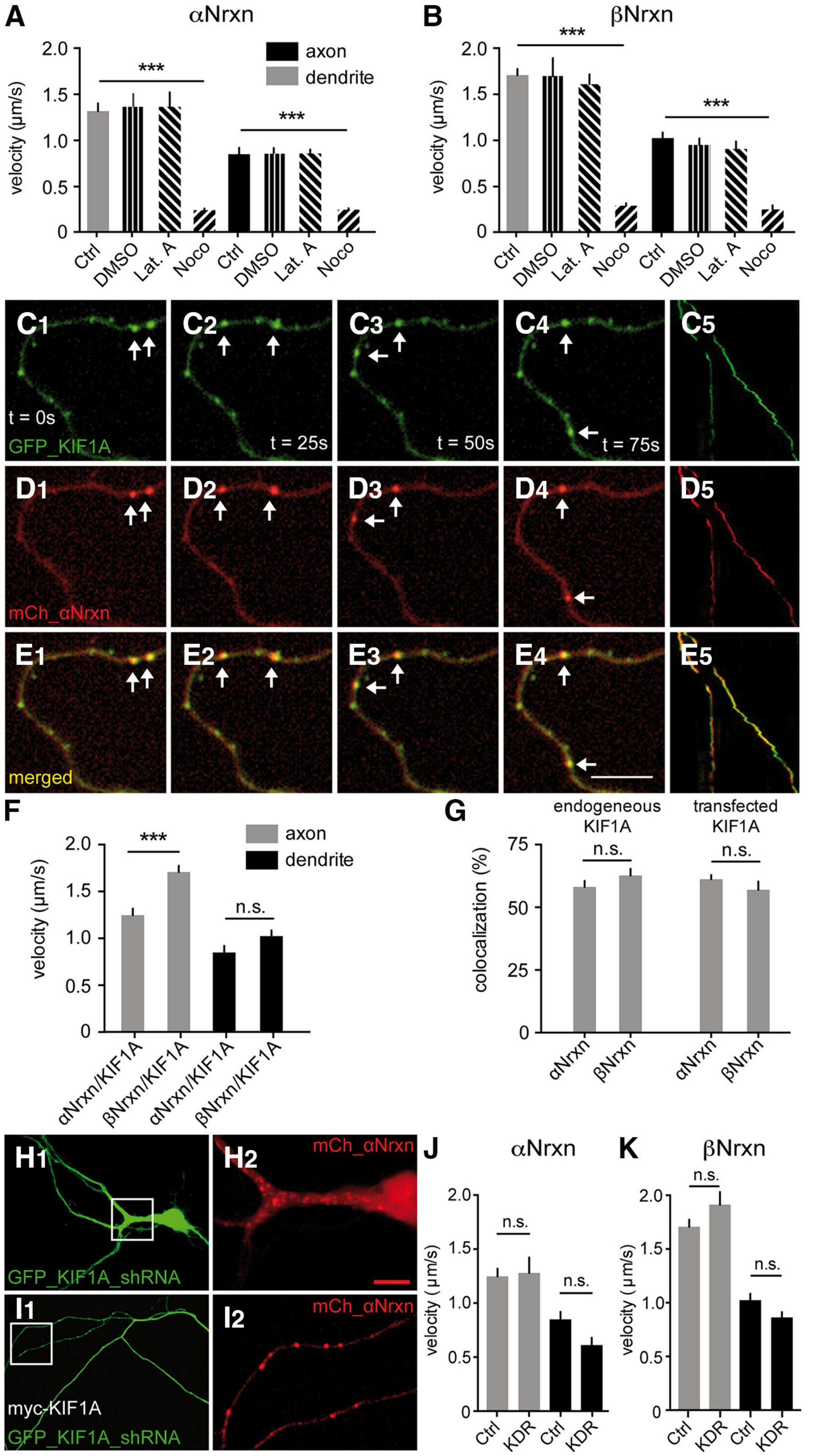

Figure 7. αNrxn and βNrxn transport depends on the microtubule motor protein KIF1A. ***A***, ***B***, Average velocities of Nrxn1α$^+$ and Nrxn1β$^+$ STVs under control conditions and after preincubation with DMSO (solvent control), latrunculin-A, and nocodazol to block F-actin (LatA) or microtubule (Noco) polymerization. ***C***–***F***, Nrxn$^+$ STVs comigrate with transfected GFP_KIF1A at velocities similar to Nrxn/synaptophysin vesicles (Fig. 6F). Scale bar, 5 μm. ***G***, High degree of colocalization between αNrxn$^+$ and βNrxn$^+$ STVs and endogenous KIF1A labeled by antibody (left bars) or transfected GFP_KIF1A (right bars). ***H***, shRNA-mediated knock-down of KIF1A (***H1***) leads to accumulation of αNrxn in soma and initial segments (***H2***). ***I***–***K***, Expression of shRNA-resistent myc-KIF1A (***I1***) is able to rescue the knock-down and reinstate localization (***I2***) and velocities of αNrxn$^+$ (***J***) and βNrxn$^+$ (***K***) STVs. Scale bar, 20 μm. Data in ***A***, ***B***, ***F***, ***G***, ***J***, and ***K*** are expressed as means ± SEM and were derived from a total of >264 neurons/27 transfected cultures. Statistical significance was tested by Student's *t* test. ***$p < 0.001$.

βNrxn/KIF1A$^+$ vesicles mimicked the values for Nrxn/synaptophysin comigration, confirming the faster speed of βNrxn-STVs in axons (Fig. 7*F*).

To prove directly that KIF1A is the molecular motor responsible for moving Nrxns, we used a combined knock-down/rescue strategy described previously (Xue et al., 2010; Liu et al., 2012). Transfecting this shRNA against KIF1A, we knocked down the protein in our primary neurons (data not shown), causing Nrxn$^+$ STVs to accumulate in the soma and axon initial segments of neurons expressing the shRNA (Fig. 7*H*). To ensure that this was not an off-target effect, we rescued the knock-down phenotype with a myc-tagged KIF1A resistant to the shRNA (Fig. 7*I1*). Under rescue conditions (KDR), Nrxn$^+$ STVs distributed normally into neurites (Fig. 7*I2*) and migrated with velocities indistinguishable from control cells (Fig. 7*J*,*K*). Together, these data indicate that Nrxn$^+$ STVs and βNrxn$^+$ STVs use the fast-microtubule-dependent transport to move toward synapses. This leaves the question of where Nrxn$^+$ STVs are inserted into the plasma membrane and how they are delivered to synaptic terminals.

Nrxns enrich at excitatory and inhibitory synapses after surface delivery

To show that Nrxn$^+$ STVs actually fuse with the plasma membrane, we used pHluorin-tagged αNrxns. We selected regions of transfected processes for FRAP, bleached large areas by short laser pulses, and monitored the spontaneous appearance of surface Nrxns by live imaging at 2–10 Hz for 5–20 min (Fig. 8*A*,*B*). At different time points during image sequences, we observed sharp increases of fluorescence intensity with longer decay (Fig. 8*B*). To determine whether these events actually corresponded to fusion of Nrxn$^+$ STVs, we monitored in parallel the appearance of pHluorin_Nrxn and pHTomato_synaptophysin cotransfected into neurons (Fig. 8*C*). In virtually all cases recorded, the increase in Nrxn fluorescence was accompanied by an increase of synaptophysin and vice versa, overlapping precisely in location and kinetics (Fig. 8*D*). Because Nrxn and synaptophysin were strictly colocalized in large fusion events, we used pHTomato_synaptophysin in combination with the Ca^{2+} indicator dye GCaMP6f (Chen et al., 2013) to determine whether STVs reached the plasma membrane at active synaptic terminals, identified by Ca^{2+} influx upon stimulation (Fig. 8*E*,*F*). Interestingly, synaptophysin$^+$ STVs appeared to fuse mostly outside of active synapses because we did not see clear overlap of Ca^{2+} signals and STV fusion (Fig. 8*G*,*H*). It should be noted, however, that the use of pHTomato, which has a lower dynamic range than pHluorin, to detect surface synaptophysin or Nrxn likely biased this analysis toward large, full-collapse fusion events. It cannot be excluded at present that additional smaller or more transient fusion events also contribute to the surface delivery of STVs and Nrxns, possibly also within synapses. Due to the high surface mobility and only transient confinement in synaptic terminals (Fig. 2), a direct insertion of Nrxn$^+$ STVs into the active zones may not be necessary to deliver Nrxn. Therefore, we propose that a combination of intracellular transport, STV fusion events outside of synaptic terminals, and distribution via lateral diffusion, with all three steps intricately regulated, targets Nrxn to synapses.

Such a scenario raises the question of if and how strongly αNrxns and βNrxns enrich at synapses. For this, we compared the relative amounts of αNrxns, βNrxns, and the Nxph1/αNrxn complex at excitatory and inhibitory terminals normalized to extrasynaptic sites of transfected axons (Fig. 9*A*). We noticed that βNrxns got more enriched than αNrxns at excitatory synapses and cotransfected Nxph1 caused an enrichment of its complex with αNrxns that exceeded the effect of αNrxns or βNrxns alone (Fig. 9*B*). In addition, we found that both Nrxns enriched threefold at inhibitory synapses and accumulation was strongest for the Nxph1/αNrxn complex (Fig. 9*B*). These results suggest that a lower surface mobility, as determined for the complex above (Figs. 2, 3, 4), does not limit its presence or enrichment in synapses. Therefore, in addition to securing delivery of sufficient molecules to terminals by lateral diffusion, the distinct surface mobilities inside synapses found above may also point to direct effects on synaptic function.

Synaptic enrichment of Nxph1/αNrxn affects $GABA_A$Rs

To study how the Nxph1/αNrxn complex, which was most distinctive in surface mobility (Fig. 2) and synaptic enrichment (Fig. 9), may exert an effect on synaptic function, we analyzed changes in postsynaptic receptor distribution. We chose the Nxph1/αNrxn complex because we showed recently that transgenic expression of Nxph1 at excitatory synapses, which normally do not contain this ligand, is able to change synaptic short-term plasticity (Born et al., 2014). Because we observed more functional $GABA_A$R at transgenic synapses in that study (Born et al., 2014), we now tested directly the ability of Nxph1/αNrxn to recruit $GABA_A$R subunits at inhibitory and excitatory terminals compared with uncomplexed αNrxns (Fig. 10). To monitor the accumulation of $GABA_A$R in primary hippocampal neurons, we first labeled the surface population of these receptors in VGAT$^-$ and VGlut1$^+$ synapses (Fig. 10*A*). The Nxph1/αNrxn complex was able to accumulate $GABA_A$Rγ2 subunits about twofold at inhibitory synapses (Fig. 10*B*). Nxph1/αNrxn was more efficient in this process than αNrxns alone (Fig. 10*C*,*D*), reflecting their differences in surface mobility (Fig. 2) and synaptic enrichment (Fig. 9). Consistently, Nxph1/αNrxn recruited $GABA_A$R also ectopically to excitatory terminals in primary neurons (Fig. 10*B*), underscoring our recent data from transgenic mice (Born et al., 2014).

Finally, we performed SPT experiments to determine whether Nxph1/αNrxn affects the diffusion dynamics of $GABA_A$R, an important parameter that has been linked to synaptic plasticity (Bannai et al., 2009). Using an antibody directed against the extracellular domain of the γ-subunit of $GABA_A$Rs, as in the earlier study (Bannai et al., 2009), we monitored the diffusion properties of endogenous $GABA_A$R in synapses. We compared the effect of expressing αNrxns or the Nxph1/αNrxn complex on surface mobility of $GABA_A$Rs colocalizing with active synaptic terminals (Fig. 10*E*). Coexpression of Nxph1/αNrxn(+SS4) strongly reduced the diffusion coefficient of $GABA_A$Rs, whereas expression of αNrxn(+SS4) alone only revealed a tendency toward reduced surface mobility. Interestingly, variants without the insert in SS4, Nxph1/αNrxn(−SS4) and αNrxn(−SS4), did not alter the surface mobility of $GABA_A$Rs (Fig. 10*E*), possibly reflecting preference for other interaction partners such as α-dystroglycan (Reissner et al., 2014). Together, our results indicate that the dynamic trafficking and synaptic enrichment of Nxph1/αNrxn may have effects on $GABA_A$R and possibly other postsynaptic receptors.

Discussion

Using single-particle tracking and time-lapse imaging, we explored the dynamic trafficking of Nrxns outside and inside of synapses and during intracellular transport to the surface. We studied overexpressed, epitope-tagged Nrxn/Nxph1 molecules because no antibodies are available against endogenous proteins that would allow these experiments. Any such approach has to

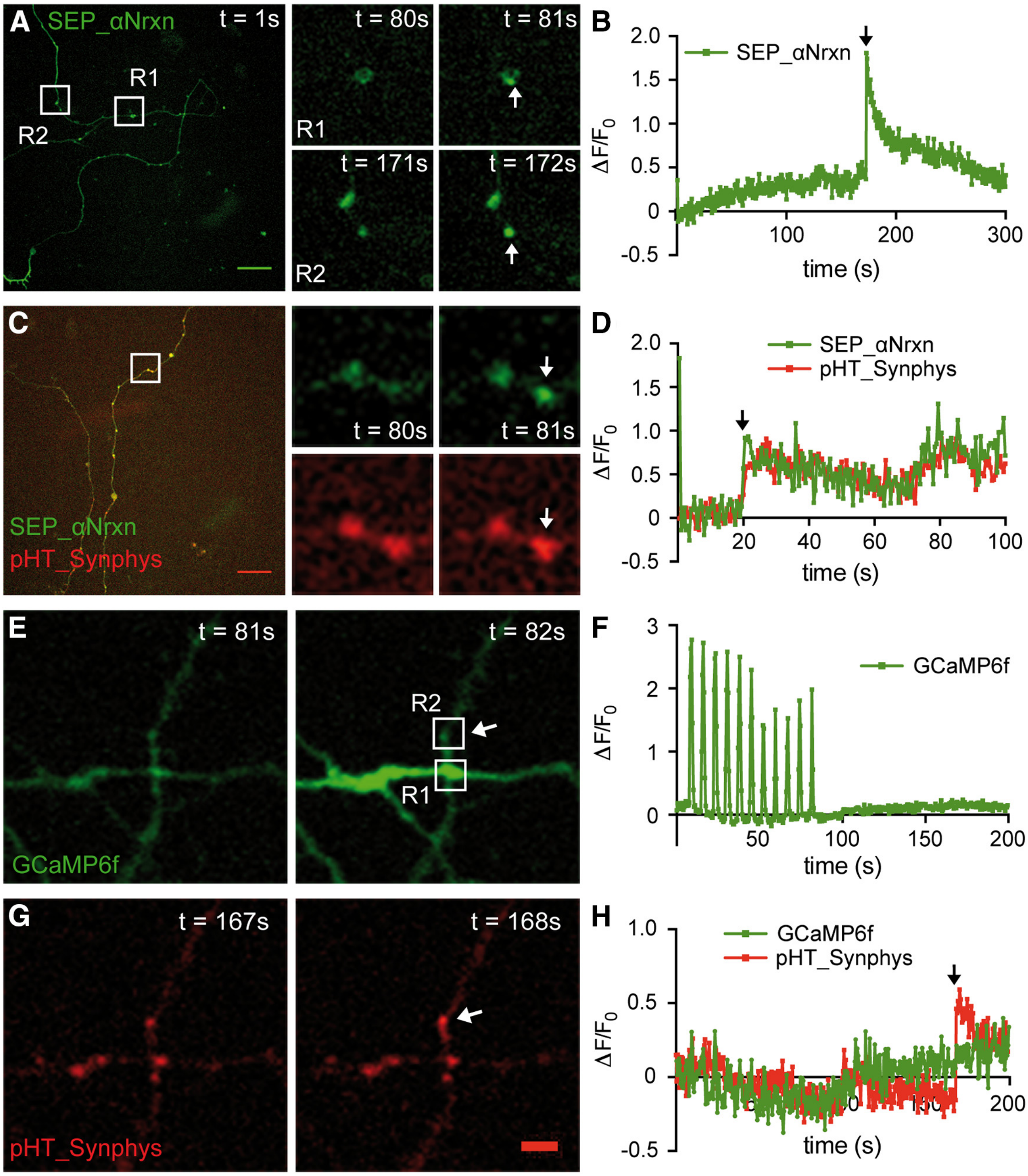

Figure 8. Synchronous surface delivery of Nrxn and synaptophysin outside of active terminals. ***A***, ***B***, Sample images of spontaneous plasma membrane fusion of pHluorin(SEP)_Nrxn1α in two different regions (R1, R2) on an axon of transfected primary neurons. The fusion events occur at different time points after bleaching the area with a 405 nm laser (FRAP). Scale bar, 20 μm. Changes of fluorescence intensity over time were recorded at DIV14 and expressed as $\Delta F/F_0$ after substraction of background, facilitating recognition of fusion events (***B***). ***C***, ***D***, In neurons cotransfected with pHluorin_Nrxn1α and pHTomato_synaptophysin (***C***), both molecules appear simultaneously and with similar kinetics at the axonal surface (***D***), indicating fusion of αNrxn/synaptophysin$^+$ STVs. ***E***–***H***, GCaMP6f Ca^{2+} indicator (***E***) and pHTomato_synaptophysin (***G***) cotransfected into primary neurons. Changes of fluorescence intensity over time reliably detect Ca^{2+} influx upon repetitive stimulation (***F***; recorded from R1). Fusion events of STVs appeared outside of active terminals and independent of stimulation/ Ca^{2+} influx (***H***; recorded from R2, arrow labels STV fusion). Scale bar, 5 μm.

consider that epitope tagging and/or overexpression may produce artifacts or limit the conclusions derived from those experiments. Therefore, we addressed the following, possibly confounding aspects. First, the surface mobility of Nrxns was tested with differently sized epitope tags (EGFP, Flag) and attached fluorophores (QDs, nanobodies) because larger molecular complexes may bias mobility (Fig. 1). Interestingly, we observed that all methods applied reliably revealed a highly mobile population of αNrxns on axons as well as within synapses. However, nanobodies showed a slightly more homogeneous distribution of diffusion in synapses, whereas QD tracking typically revealed a second, more immobile population, which is also apparent in the analyses shown in Figure 2 (e.g., Fig. 2*E* or *K*). Despite this small additional population, the QD data turned out to be robust enough to reveal clear and significant differences between Nrxn variants or between extrasynaptic regions and glutamatergic or GABAergic terminals (Figs. 2, 3, 4). Future research will have to explore whether the presence of an additional, more immobile Nrxn population was due to size limitations of QD tracking within synaptic terminals or to a bias of nanobody tracking toward higher mobilities.

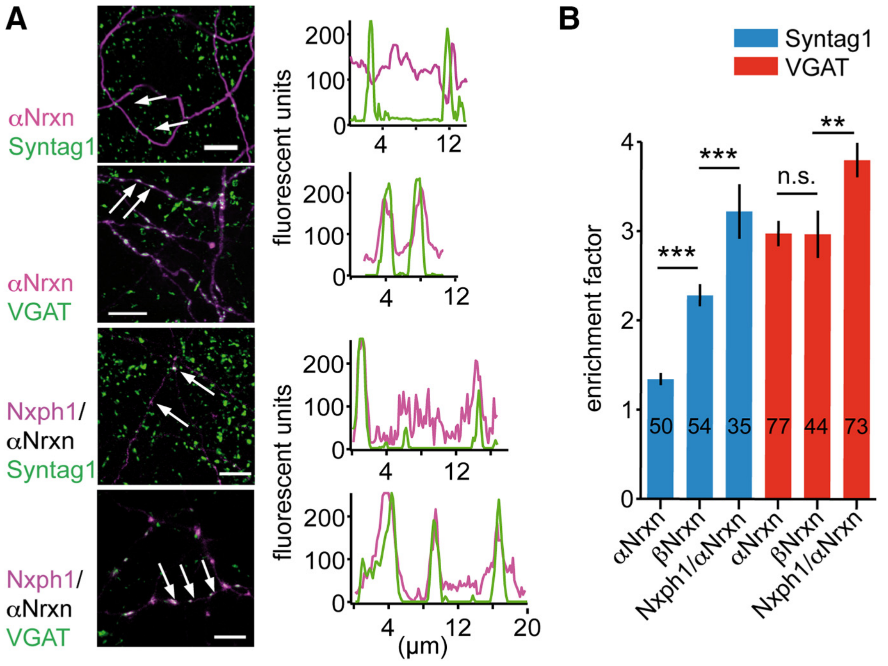

Figure 9. Enrichment of Nrxns and the Nxph1/αNrxn complex at synapses. ***A***, Sample images of pHluorin(SEP)_Nrxn1α$^+$ axons of glutamatergic and GABAergic neurons. Strong accumulation of αNrxns seen at VGAT/Syntag1$^+$ putatively inhibitory terminals compared with Syntag1$^+$ putatively excitatory synapses is supported by corresponding line scans (right panels). Scale bar, 10 μm. ***B***, Enrichment of αNrxns, βNrxns, and the Nxph1/αNrxn complex at excitatory (blue) and inhibitory (red) synapses normalized to extrasynaptic axonal sites (set to 1). Data are means ± SEM and were collected from 3 different cultures for each construct with number of analyzed synapses indicated in bars. Statistical significance was tested by a one-way ANOVA test followed by a Keuls–Newman post test. ***$p < 0.0001$, **$p < 0.001$.

Second, similar to the analysis of surface mobility, we used different epitopes (EGFP, mCherry, HRP) in this and a previous study to investigate the intracellular transport of Nrxns. In addition, we have previously tested different positions within the Nrxn molecules (N terminus, extracellular to transmembrane region). These experiments all demonstrated that Nrxns are transported as cargo on STVs (Figs. 5, 6; Fairless et al., 2008). Moreover, the choice of EGFP or mCherry did not affect the velocity of Nrxn-positive STVs (Figs. 5, 6).

Third, to validate our data on Nrxn surface mobility with another method and to compare our data with published results, we performed a set of FRAP experiments. We found that the fraction of mobile Nrxn molecules was comparable between SPT and FRAP measurements (Fig. 1) and between cultured primary neurons (Fig. 1) and slice cultures (Fu and Huang, 2010).

Finally, we tried to determine how much the overexpression of tagged Nrxns influenced our results, arguably the most difficult variable to assess. The comparable surface mobilities derived from FRAP (Fig. 1; Fu and Huang, 2010) and SPT experiments (Fig. 2) suggest that the level and mode of overexpression (transgenic mice vs transfection) did not alter the diffusion coefficient nor the fraction of mobile molecules. In addition, we observed that the removal of endogenous αNrxns reduced the diffusion rates of transfected αNrxn variants in TKO neurons, but did not abolish the presence of highly mobile αNrxns (Fig. 2). This result was expected if transfected Nrxns engage in normal protein–protein interactions because more ligands may be available in the TKO to interact. The reduction in the diffusion coefficient actually demonstrates that transfected, overexpressed Nrxns behave like endogenous Nrxns by taking their positions. This is supported by our finding that prevention of such interactions leads to higher mobilities (Fig. 3). For the intracellular transport of αNrxns, we have previously shown that it is largely independent of endogenous protein (Fairless et al., 2008). In support, our current analysis reveals that the velocity of αNrxn$^+$ STVs is indistinguishable between WT and TKO neurons (Fig. 6). Finally, important previous studies have used overexpressed Nrxns extensively to unravel their functions, for example, in synapse formation assays that revealed the role of Nrxn in differentiating novel contacts (Graf et al., 2004; Boucard et al., 2005; Nam and Chen, 2005; Chih et al., 2006). Therefore, based on our controls and published evidence, we believe that overexpressed, epitope-tagged Nrxns are an acceptable tool to study their dynamic trafficking.

We first observed a higher surface mobility of αNrxns compared with βNrxns (Fig. 2), which is an unexpected result in view of the much longer and rigid extracellular domains of αNrxns (Chen et al., 2011; Miller et al., 2011). These results agree with a study in slice cultures from transgenic mice that proposed a higher population mobility for αNrxns by FRAP (Fu and Huang, 2010). Our data are also consistent with a diffusion coefficient for βNrxns determined in slice cultures (Biermann et al., 2014) that was only moderately slower compared with primary neurons (Fig. 2). In addition, the value determined here for extrasynaptic αNrxn on axonal membranes ($D \approx 0.07\ \mu m^2/s$) is comparable to other neuronal adhesion molecules with long extracellular domains such as SynCAM ($D \approx 0.05\ \mu m^2/s$) or *N*-cadherin ($D \approx 0.08\ \mu m^2/s$; Heine, 2012). Therefore, the faster diffusion dynamics of αNrxns compared with βNrxns indicates that size-dependent passive mechanisms are not critical for surface mobility.

In contrast, we demonstrate that Ca^{2+}- and SS4-dependent interactions are regulators of Nrxn surface mobility (Figs. 2, 3). Although the list of identified binding partners is likely not complete, neuroligins, LRRTMs, and dystroglycan (Ichtchenko et al., 1995; Ichtchenko et al., 1996; Sugita et al., 2001; Reissner et al., 2008; Ko et al., 2009; Siddiqui et al., 2010; Reissner et al., 2014), and possibly also calsyntenin-3 (Pettem et al., 2013; Lu et al., 2014; Um et al., 2014), are known to require Ca^{2+} for their interaction. Binding affinities are further regulated by splice site SS4 because neuroligins, LRRTMs, and dystroglycan favor insertless and cerebellin insert-containing variants (Ichtchenko et al., 1995; Sugita et al., 2001; Boucard et al., 2005; Reissner et al., 2008; Ko et al., 2009; de Wit et al., 2009b; Koehnke et al., 2010; Uemura et al., 2010; Joo et al., 2011; Matsuda and Yuzaki, 2011; Lee et al., 2012; Reissner et al., 2014). The fact that known splice-variant-dependent binding properties of Nrxns are reflected by differences in mobility (Fig. 3) underscores the importance of alternative splicing and transcriptional regulation (Chih et al., 2006; Iijima et al., 2011; Aoto et al., 2013; Ehrmann et al., 2013; Runkel et al., 2013; Treutlein et al., 2014).

We also reveal that the surface mobility of αNrxns is modulated by complex formation with Nxph1 (Missler et al., 1998). In contrast to αNrxns (Ullrich et al., 1995), Nxphs are only expressed by subpopulations of neurons (Petrenko et al., 1996; Beglopoulos et al., 2005). Our observation that efficient surface targeting of Nxph1 requires coexpression with αNrxna (Fig. 4), but not vice versa, constitutes an asymmetric dependence. This asymmetry unveils a surprising twist because initial sequence analysis, which identified a signal peptide, preprodomain, and a bibasic proteolytic cleavage site, suggested independently secreted Nxph (Petrenko et al., 1996; Missler and Südhof, 1998; Missler et al., 1998). Recent data from transgenic overexpression of Nxph1 showed alterations of synaptic function and ectopic accumulation of functional GABA$_A$R subunits (Born et al., 2014). Given the asymmetric dependence on αNrxns (Fig. 4), the transgenic Nxph1 phenotype might be based on the slow diffusion and longer dwell time of Nxph1/αNrxn complexes (Fig. 2). Accordingly, biochemical data showed that complex formation between the LNS2 domain of αNrxn with Nxph1 is mutually exclusive with α-dystroglycan, and thus favors association with particular Nlgn variants at the LNS6 domain (Reissner et al., 2014). This in turn may decrease the surface mobility (Figs. 2, 3).

Enrichment of Nxph1/αNrxn at terminals led to recruitment and stabilization of endogenous GABA$_A$R subunits in transfected synapses (Figs. 9, 10), consistent with Nxph1 overexpression in transgenic mice (Born et al., 2014). The stronger effect found in presence of Nxph1/αNrxn compared with αNrxns and at inhibitory compared with excitatory synapses (Fig. 10), mirrors the difference in their surface mobilities (Fig. 2). In agreement, αNrxns expressed in heterologous cells induced clustering of GABA$_A$R subunits in contacting dendrites (Graf et al., 2004; Kang et al., 2008) and inhibitory synapses were reduced in TKO (Dudanova et al., 2007). In addition, Nrxns were linked to postsynaptic GABA$_A$R function in lentivirus-mediated knock-down experiments in primary neurons (Zhang et al., 2010). Therefore, the recruitment of GABA$_A$R and the down-regulation of its diffusion dynamics by Nxph1/αNrxn demonstrates that the complex can shape synaptic function.

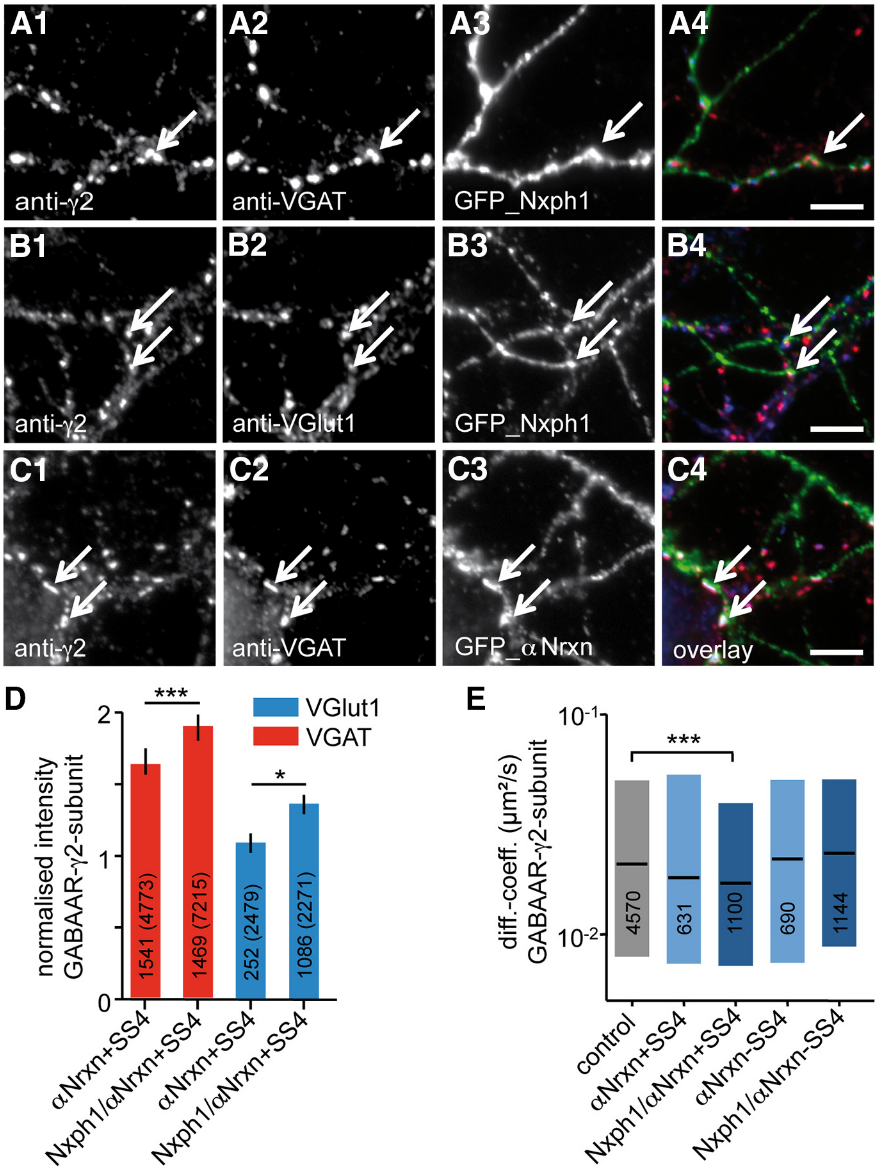

Figure 10. αNrxns and the Nxph1/αNrxn complex are effective in recruiting GABA$_A$R subunits to synapses. ***A–C***, Primary hippocampal neurons transfected with the pHluorin(SEP)_Nxph1/αNrxn complex or SEP_αNrxns alone are colabeled against GABA$_A$Rγ2, and VGAT or VGlut1 to distinguish inhibitory from excitatory terminals. Scale bar, 10 μm. ***D***, αNrxns and the Nxph1/αNrxn complex cause enrichment of GABA$_A$Rγ2 subunits at inhibitory synapses (red) and Nxph1/αNrxn also at excitatory synapses (blue). Data are shown as means ± SEM, with the number of analyzed transfected and nontransfected (in paranthesis) synapses shown in bars. Statistical significance was tested by one-way ANOVA variance test followed by Newman–Keuls test. $*p < 0.05$, $***p < 0.0001$. ***E***, SPT with QD-labeled antibodies against endogenous GABA$_A$Rγ2 on axons of neurons transfected with αNrxns or the Nxph1/αNrxn complex (± insert at SS4). Coexpression of Nxph1 decreases diffusion coefficients of GABA$_A$Rγ when the insert is present in αNrxn (+SS4). Data are shown as median plus IQR (25–75%) and were collected from 3 independent cultures. Significance was tested by a Kruskal–Wallis test followed by a Dunn's test. $***p < 0.0001$.

Although the diffusion coefficient of Nrxns is considerably high, diffusion is only effective at short distances (Rusakov et al., 2011), for example, within synaptic terminals or their immediate vicinity. We therefore hypothesized that neurons rely on fast intracellular transport of Nrxns and discovered that they are transported as cargo via typical STVs (Figs. 5, 6, 7). Unlike surface mobility, βNrxn$^+$ STVs moved faster than αNrxn$^+$ STVs within axons (Fig. 6), possibly because smaller βNrxns can assemble more densely in sheet-like superstructures (Tanaka et al., 2012), providing more access for their molecular motor KIF1A (Fig. 7). Velocities of 1–2 μm/s appear sufficient to deliver Nrxn$^+$ STVs even to distant terminals, in particular because increased neuronal activity could augment speed (Fig. 6). Therefore, the combination of fast intracellular transport via STVs, fusion near active synapses (Fig. 8), and lateral diffusion on the surface appears ideally suited to maintain and modulate the amount of Nrxn variants at synapses. Future work will have to address how their dynamic trafficking affects synaptic function.

References

Ahmari SE, Buchanan J, Smith SJ (2000) Becausesembly of presynaptic active zones from cytoplasmic transport packets. Nat Neurosci 3:445–451. CrossRef Medline

Anggono V, Huganir RL (2012) Regulation of AMPA receptor trafficking and synaptic plasticity. Curr Opin Neurobiol 22:461–469. CrossRef Medline

Aoto J, Martinelli DC, Malenka RC, Tabuchi K, Südhof TC (2013) Presynaptic neurexin-3 alternative splicing trans-synaptically controls postsynaptic AMPA receptor trafficking. Cell 154:75–88. CrossRef Medline

Bannai H, Lévi S, Schweizer C, Inoue T, Launey T, Racine V, Sibarita JB, Mikoshiba K, Triller A (2009) Activity-dependent tuning of inhibitory neurotransmission based on GABAAR diffusion dynamics. Neuron 62:670–682. CrossRef Medline

Beglopoulos V, Montag-Sallaz M, Rohlmann A, Piechotta K, Ahmad M, Montag D, Missler M (2005) Neurexophilin 3 is highly localized in cortical and cerebellar regions and is functionally important for sensorimotor gating and motor coordination. Mol Cell Biol 25:7278–7288. CrossRef Medline

Biermann B, Ivankova-Susankova K, Bradaia A, Abdel Aziz S, Besseyrias V, Kapfhammer JP, Missler M, Gassmann M, Bettler B (2010) The Sushi domains of GABAB receptors function as axonal targeting signals. J Neurosci 30:1385–1394. CrossRef Medline

Biermann B, Sokoll S, Klueva J, Missler M, Wiegert JS, Sibarita JB, Heine M (2014) Imaging of molecular surface dynamics in brain slices using single-particle tracking. Nat Commun 5:3024. Medline

Born G, Breuer D, Wang S, Rohlmann A, Coulon P, Vakili P, Reissner C, Kiefer F, Heine M, Pape HC, Missler M (2014) Modulation of synaptic function through the alpha-neurexin-specific ligand neurexophilin-1. Proc Natl Acad Sci U S A 111:E1274–1283. CrossRef Medline

Born G, Grayton HM, Langhorst H, Dudanova I, Rohlmann A, Woodward BW, Collier DA, Fernandes C, Missler M (2015) Genetic targeting of NRXN2 in mice unveils role in excitatory cortical synapse function and social behaviors. Front Synaptic Neurosci 7:3. Medline

Bottos A, Rissone A, Bussolino F, Arese M (2011) Neurexins and neuroligins: synapses look out of the nervous system. Cell Mol Life Sci 68:2655–2666. CrossRef Medline

Boucard AA, Chubykin AA, Comoletti D, Taylor P, Südhof TC (2005) A splice code for trans-synaptic cell adhesion mediated by binding of neuroligin 1 to alpha- and beta-neurexins. Neuron 48:229–236. CrossRef Medline

Boucard AA, Ko J, Südhof TC (2012) High affinity neurexin binding to cell adhesion G-protein-coupled receptor CIRL1/latrophilin-1 produces an intercellular adhesion complex. J Biol Chem 287:9399–9413. CrossRef Medline

Budreck EC, Kwon OB, Jung JH, Baudouin S, Thommen A, Kim HS, Fukazawa Y, Harada H, Tabuchi K, Shigemoto R, Scheiffele P, Kim JH (2013) Neuroligin-1 controls synaptic abundance of NMDA-type glutamate receptors through extracellular coupling. Proc Natl Acad Sci U S A 110:725–730. CrossRef Medline

Bury LA, Sabo SL (2011) Coordinated trafficking of synaptic vesicle and active zone proteins prior to synapse formation. Neural Dev 6:24. CrossRef Medline

Chang JC, Tomlinson ID, Warnement MR, Ustione A, Carneiro AM, Piston DW, Blakely RD, Rosenthal SJ (2012) Single molecule analysis of serotonin transporter regulation using antagonist-conjugated quantum dots reveals restricted, p38 MAPK-dependent mobilization underlying uptake activation. J Neurosci 32:8919–8929. CrossRef Medline

Chen F, Venugopal V, Murray B, Rudenko G (2011) The structure of neurexin 1alpha reveals features promoting a role as synaptic organizer. Structure 19:779–789. CrossRef Medline

Chen JL, Villa KL, Cha JW, So PT, Kubota Y, Nedivi E (2012) Clustered dynamics of inhibitory synapses and dendritic spines in the adult neocortex. Neuron 74:361–373. CrossRef Medline

Chen TW, Wardill TJ, Sun Y, Pulver SR, Renninger SL, Baohan A, Schreiter ER, Kerr RA, Orger MB, Jayaraman V, Looger LL, Svoboda K, Kim DS (2013) Ultrasensitive fluorescent proteins for imaging neuronal activity. Nature 499:295–300. CrossRef Medline

Chia PH, Li P, Shen K (2013) Cell biology in neuroscience: cellular and molecular mechanisms underlying presynapse formation. J Cell Biol 203:11–22. CrossRef Medline

Chih B, Gollan L, Scheiffele P (2006) Alternative splicing controls selective trans-synaptic interactions of the neuroligin-neurexin complex. Neuron 51:171–178. CrossRef Medline

Cijsouw T, Weber JP, Broeke JH, Broek JA, Schut D, Kroon T, Saarloos I, Verhage M, Toonen RF (2014) Munc18–1 redistributes in nerve terminals in an activity- and PKC-dependent manner. J Cell Biol 204:759–775. CrossRef Medline

Dean C, Scholl FG, Choih J, DeMaria S, Berger J, Isacoff E, Scheiffele P (2003) Neurexin mediates the assembly of presynaptic terminals. Nat Neurosci 6:708–716. CrossRef Medline

de Wit J, Toonen RF, Verhaagen J, Verhage M (2006) Vesicular trafficking of semaphorin 3A is activity-dependent and differs between axons and dendrites. Traffic 7:1060–1077. CrossRef Medline

de Wit J, Toonen RF, Verhage M (2009a) Matrix-dependent local retention of secretory vesicle cargo in cortical neurons. J Neurosci 29:23–37. CrossRef Medline

de Wit J, Sylwestrak E, O'Sullivan ML, Otto S, Tiglio K, Savas JN, Yates JR 3rd, Comoletti D, Taylor P, Ghosh A (2009b) LRRTM2 interacts with Neurexin1 and regulates excitatory synapse formation. Neuron 64:799–806. CrossRef Medline

Di Biase V, Tuluc P, Campiglio M, Obermair GJ, Heine M, Flucher BE (2011) Surface traffic of dendritic CaV1.2 calcium channels in hippocampal neurons. J Neurosci 31:13682–13694. CrossRef Medline

Dobie FA, Craig AM (2011) Inhibitory synapse dynamics: coordinated presynaptic and postsynaptic mobility and the major contribution of recycled vesicles to new synapse formation. J Neurosci 31:10481–10493. CrossRef Medline

Dolphin AC (2012) Calcium channel auxiliary alpha2delta and beta subunits: trafficking and one step beyond. Nat Rev Neurosci 13:542–555. Medline

Dudanova I, Tabuchi K, Rohlmann A, Südhof TC, Missler M (2007) Deletion of alpha-neurexins does not cause a major impairment of axonal pathfinding or synapse formation. J Comp Neurol 502:261–274. CrossRef Medline

Dupuis JP, Ladépêche L, Seth H, Bard L, Varela J, Mikasova L, Bouchet D, Rogemond V, Honnorat J, Hanse E, Groc L (2014) Surface dynamics of GluN2B-NMDA receptors controls plasticity of maturing glutamate synapses. EMBO J 33:842–861. CrossRef Medline

Ehrmann I, Dalgliesh C, Liu Y, Danilenko M, Crosier M, Overman L, Arthur HM, Lindsay S, Clowry GJ, Venables JP, Fort P, Elliott DJ (2013) The tissue-specific RNA binding protein T-STAR controls regional splicing patterns of neurexin pre-mRNBecause in the brain. PLoS Genet 9:e1003474. CrossRef Medline

Ermolyuk YS, Alder FG, Henneberger C, Rusakov DA, Kullmann DM, Volynski KE (2012) Independent regulation of basal neurotransmitter release efficacy by variable Ca(2)+ influx and bouton size at small central synapses. PLoS Biol 10:e1001396. CrossRef Medline

Etherton MR, Blaiss CA, Powell CM, Südhof TC (2009) Mouse neurexin-1alpha deletion causes correlated electrophysiological and behavioral changes consistent with cognitive impairments. Proc Natl Acad Sci U S A 106:17998–18003. CrossRef Medline

Fairless R, Masius H, Rohlmann A, Heupel K, Ahmad M, Reissner C, Dresbach T, Missler M (2008) Polarized targeting of neurexins to synapses is regulated by their C-terminal sequences. J Neurosci 28:12969–12981. CrossRef Medline

Fu Y, Huang ZJ (2010) Differential dynamics and activity-dependent regulation of alpha- and beta-neurexins at developing GABAergic synapses. Proc Natl Acad Sci U S A 107:22699–22704. CrossRef Medline

Giannone G, Mondin M, Grillo-Bosch D, Tessier B, Saint-Michel E, Czöndör K, Sainlos M, Choquet D, Thoumine O (2013) Neurexin-1beta binding to neuroligin-1 triggers the preferential recruitment of PSD-95 versus gephyrin through tyrosine phosphorylation of neuroligin-1. Cell Rep 3:1996–2007. CrossRef Medline

Gokce O, Südhof TC (2013) Membrane-tethered monomeric neurexin LNS-domain triggers synapse formation. J Neurosci 33:14617–14628. CrossRef Medline

Graf ER, Zhang X, Jin SX, Linhoff MW, Craig AM (2004) Neurexins induce differentiation of GABA and glutamate postsynaptic specializations via neuroligins. Cell 119:1013–1026. CrossRef Medline

Groc L, Lafourcade M, Heine M, Renner M, Racine V, Sibarita JB, Lounis B, Choquet D, Cognet L (2007) Surface trafficking of neurotransmitter receptor: comparison between single-molecule/quantum dot strategies. J Neurosci 27:12433–12437. CrossRef Medline

Heine M (2012) Surface traffic in synaptic membranes. Adv Exp Med Biol 970:197–219. CrossRef Medline

Heine M, Thoumine O, Mondin M, Tessier B, Giannone G, Choquet D (2008a) Activity-independent and subunit-specific recruitment of functional AMPA receptors at neurexin/neuroligin contacts. Proc Natl Acad Sci U S A 105:20947–20952. CrossRef Medline

Heine M, Groc L, Frischknecht R, Béïque JC, Lounis B, Rumbaugh G, Huganir RL, Cognet L, Choquet D (2008b) Surface mobility of postsynaptic AMPARs tunes synaptic transmission. Science 320:201–205. CrossRef Medline

Hirokawa N, Noda Y, Tanaka Y, Niwa S (2009) Kinesin superfamily motor proteins and intracellular transport. Nat Rev Mol Cell Biol 10:682– 696. Medline

Ichtchenko K, Hata Y, Nguyen T, Ullrich B, Missler M, Moomaw C, Südhof TC (1995) Neuroligin 1: a splice site-specific ligand for beta-neurexins. Cell 81:435– 443. CrossRef Medline

Ichtchenko K, Nguyen T, Südhof TC (1996) Structures, alternative splicing, and neurexin binding of multiple neuroligins. J Biol Chem 271:2676 –2682. CrossRef Medline

Iijima T, Wu K, Witte H, Hanno-Iijima Y, Glatter T, Richard S, Scheiffele P (2011) SAM68 regulates neuronal activity-dependent alternative splicing of neurexin-1. Cell 147:1601–1614. CrossRef Medline

Joo JY, Lee SJ, Uemura T, Yoshida T, Yasumura M, Watanabe M, Mishina M (2011) Differential interactions of cerebellin precursor protein (Cbln) subtypes and neurexin variants for synapse formation of cortical neurons. Biochem Biophys Res Commun 406:627– 632. CrossRef Medline

Kaech S, Banker G (2006) Culturing hippocampal neurons. Nat Protoc 1:2406 –2415. CrossRef Medline

Kang Y, Zhang X, Dobie F, Wu H, Craig AM (2008) Induction of GABAergic postsynaptic differentiation by alpha-neurexins. J Biol Chem 283: 2323–2334. CrossRef Medline

Kattenstroth G, Tantalaki E, Südhof TC, Gottmann K, Missler M (2004) Postsynaptic N-methyl-D-aspartate receptor function requires alpha-neurexins. Proc Natl Acad Sci U S A 101:2607–2612. CrossRef Medline

Kechkar A, Nair D, Heilemann M, Choquet D, Sibarita JB (2013) Real-time analysis and visualization for single-molecule based super-resolution microscopy. PLoS One 8:e62918. CrossRef Medline

Ko J, Fuccillo MV, Malenka RC, Südhof TC (2009) LRRTM2 functions as a neurexin ligand in promoting excitatory synapse formation. Neuron 64: 791–798. CrossRef Medline

Koehnke J, Katsamba PS, Ahlsen G, Bahna F, Vendome J, Honig B, Shapiro L, Jin X (2010) Splice form dependence of beta-neurexin/neuroligin binding interactions. Neuron 67:61–74. CrossRef Medline

Kraszewski K, Mundigl O, Daniell L, Verderio C, Matteoli M, De Camilli P (1995) Synaptic vesicle dynamics in living cultured hippocampal neurons visualized with CY3-conjugated antibodies directed against the lumenal domain of synaptotagmin. J Neurosci 15:4328 – 4342. Medline

Kwon HB, Sabatini BL (2011) Glutamate induces de novo growth of functional spines in developing cortex. Nature 474:100 –104. CrossRef Medline

Lau CG, Zukin RS (2007) NMDA receptor trafficking in synaptic plasticity and neuropsychiatric disorders. Nat Rev Neurosci 8:413– 426. Medline

Lee JR, Shin H, Ko J, Choi J, Lee H, Kim E (2003) Characterization of the movement of the kinesin motor KIF1A in living cultured neurons. J Biol Chem 278:2624 –2629. CrossRef Medline

Lee SJ, Uemura T, Yoshida T, Mishina M (2012) GluRdelta2 assembles four neurexins into trans-synaptic triad to trigger synapse formation. J Neurosci 32:4688 – 4701. CrossRef Medline

Liu JS, Schubert CR, Fu X, Fourniol FJ, Jaiswal JK, Houdusse A, Stultz CM, Moores CA, Walsh CA (2012) Molecular basis for specific regulation of neuronal kinesin-3 motors by doublecortin family proteins. Mol Cell 47:707–721. CrossRef Medline

Lu Z, Wang Y, Chen F, Tong H, Reddy MV, Luo L, Seshadrinathan S, Zhang L, Holthauzen LM, Craig AM, Ren G, Rudenko G (2014) Calsyntenin-3 molecular architecture and interaction with neurexin 1alpha. J Biol Chem 289:34530 –34542. CrossRef Medline

Martens H, Weston MC, Boulland JL, Gronborg M, Grosche J, Kacza J, Hoffmann A, Matteoli M, Takamori S, Harkany T, Chaudhry FA, Rosenmund C, Erck C, Jahn R, Härtig W (2008) Unique luminal localization of VGAT-C terminus allows for selective labeling of active cortical GABAergic synapses. J Neurosci 28:13125–13131. CrossRef Medline

Matsuda K, Yuzaki M (2011) Cbln family proteins promote synapse formation by regulating distinct neurexin signaling pathways in various brain regions. Eur J Neurosci 33:1447–1461. CrossRef Medline

McAllister AK (2007) Dynamic aspects of CNS synapse formation. Annu Rev Neurosci 30:425– 450. CrossRef Medline

Miller MT, Mileni M, Comoletti D, Stevens RC, Harel M, Taylor P (2011) The crystal structure of the alpha-neurexin-1 extracellular region reveals a hinge point for mediating synaptic adhesion and function. Structure 19: 767–778. CrossRef Medline

Missler M, Südhof TC (1998) Neurexophilins form a conserved family of neuropeptide-like glycoproteins. J Neurosci 18:3630 –3638. Medline

Missler M, Hammer RE, Südhof TC (1998) Neurexophilin binding to alpha-neurexins. A single LNS domain functions as an independently folding ligand-binding unit. J Biol Chem 273:34716 –34723. CrossRef Medline

Missler M, Zhang W, Rohlmann A, Kattenstroth G, Hammer RE, Gottmann K, Südhof TC (2003) Alpha-neurexins couple Ca2+ channels to synaptic vesicle exocytosis. Nature 423:939 –948. CrossRef Medline

Missler M, Südhof TC, Biederer T (2012) Synaptic cell adhesion. Cold Spring Harb Perspect Biol 4:a005694. Medline

Mondin M, Labrousse V, Hosy E, Heine M, Tessier B, Levet F, Poujol C, Blanchet C, Choquet D, Thoumine O (2011) Neurexin-neuroligin adhesions capture surface-diffusing AMPA receptors through PSD-95 scaffolds. J Neurosci 31:13500 –13515. CrossRef Medline

Muyldermans S (2013) Nanobodies: natural single-domain antibodies. Annu Rev Biochem 82:775–797. CrossRef Medline

Nam CI, Chen L (2005) Postsynaptic assembly induced by neurexin-neuroligin interaction and neurotransmitter. Proc Natl Acad Sci U S A 102:6137– 6142. CrossRef Medline

Park JJ, Gondré-Lewis MC, Eiden LE, Loh YP (2011) A distinct trans-Golgi network subcompartment for sorting of synaptic and granule proteins in neurons and neuroendocrine cells. J Cell Sci 124:735–744. CrossRef Medline

Petrenko AG, Ullrich B, Missler M, Krasnoperov V, Rosahl TW, Südhof TC (1996) Structure and evolution of neurexophilin. J Neurosci 16:4360 – 4369. Medline

Pettem KL, Yokomaku D, Luo L, Linhoff MW, Prasad T, Connor SA, Siddiqui TJ, Kawabe H, Chen F, Zhang L, Rudenko G, Wang YT, Brose N, Craig AM (2013) The specific alpha-neurexin interactor calsyntenin-3 promotes excitatory and inhibitory synapse development. Neuron 80:113–128. CrossRef Medline

Reissner C, Klose M, Fairless R, Missler M (2008) Mutational analysis of the neurexin/neuroligin complex reveals essential and regulatory components. Proc Natl Acad Sci U S A 105:15124 –15129. CrossRef Medline

Reissner C, Runkel F, Missler M (2013) Neurexins. Genome Biol 14:213. CrossRef Medline

Reissner C, Stahn J, Breuer D, Klose M, Pohlentz G, Mormann M, Missler M (2014) Dystroglycan binding to alpha-neurexin competes with neurexophilin-1 and neuroligin in the brain. J Biol Chem 289:27585–27603. CrossRef Medline

Ribrault C, Reingruber J, Petković M, Galli T, Ziv NE, Holcman D, Triller A (2011) Syntaxin1A lateral diffusion reveals transient and local SNARE interactions. J Neurosci 31:17590 –17602. CrossRef Medline

Rozov A, Burnashev N, Sakmann B, Neher E (2001) Transmitter release modulation by intracellular Ca2+ buffers in facilitating and depressing nerve terminals of pyramidal cells in layer 2/3 of the rat neocortex indicates a target cell-specific difference in presynaptic calcium dynamics. J Physiol 531:807– 826. CrossRef Medline

Runkel F, Rohlmann A, Reissner C, Brand SM, Missler M (2013) Promoter-like sequences regulating transcriptional activity in neurexin and neuroligin genes. J Neurochem 127:36 – 47. Medline

Rusakov DA, Savtchenko LP, Zheng K, Henley JM (2011) Shaping the synaptic signal: molecular mobility inside and outside the cleft. Trends Neurosci 34:359 –369. CrossRef Medline

Sabo SL, Gomes RA, McAllister AK (2006) Formation of presynaptic terminals at predefined sites along axons. J Neurosci 26:10813–10825. CrossRef Medline

Saxton MJ (1995) Single-particle tracking: effects of corrals. Biophys J 69: 389 –398. CrossRef Medline

Schneider R, Hosy E, Kohl J, Klueva J, Choquet D, Thomas U, Voigt A, Heine M (2015) Mobility of calcium channels in the presynaptic membrane. Neuron 86:672– 679. CrossRef Medline

Schreiner D, Nguyen TM, Russo G, Heber S, Patrignani A, Ahrné E, Scheiffele P (2014) Targeted combinatorial alternative splicing generates brain region-specific repertoires of neurexins. Neuron 84:386–398. CrossRef Medline

Schreiner D, Simicevic J, Ahrne E, Schmidt A, Scheiffele P (2015) Quantitative isoform-profiling of highly diversified recognition molecules. eLife 4.

Sergé A, Fourgeaud L, Hemar A, Choquet D (2002) Receptor activation and homer differentially control the lateral mobility of metabotropic glutamate receptor 5 in the neuronal membrane. J Neurosci 22:3910–3920. Medline

Shen K, Scheiffele P (2010) Genetics and cell biology of building specific synaptic connectivity. Annu Rev Neurosci 33:473–507. CrossRef Medline

Siddiqui TJ, Pancaroglu R, Kang Y, Rooyakkers A, Craig AM (2010) LRRTMs and neuroligins bind neurexins with a differential code to cooperate in glutamate synapse development. J Neurosci 30:7495–7506. CrossRef Medline

Sugita S, Saito F, Tang J, Satz J, Campbell K, Südhof TC (2001) A stoichiometric complex of neurexins and dystroglycan in brain. J Cell Biol 154: 435–445. CrossRef Medline

Tanaka H, Miyazaki N, Matoba K, Nogi T, Iwasaki K, Takagi J (2012) Higher-order architecture of cell adhesion mediated by polymorphic synaptic adhesion molecules neurexin and neuroligin. Cell Rep 2:101–110. CrossRef Medline

Taniguchi H, Gollan L, Scholl FG, Mahadomrongkul V, Dobler E, Limthong N, Peck M, Aoki C, Scheiffele P (2007) Silencing of neuroligin function by postsynaptic neurexins. J Neurosci 27:2815–2824. CrossRef Medline

Treutlein B, Gokce O, Quake SR, Südhof TC (2014) Cartography of neurexin alternative splicing mapped by single-molecule long-read mRNA sequencing. Proc Natl Acad Sci U S A 111:E1291–1299. CrossRef Medline

Triller A, Choquet D (2008) New concepts in synaptic biology derived from single-molecule imaging. Neuron 59:359–374. CrossRef Medline

Uemura T, Lee SJ, Yasumura M, Takeuchi T, Yoshida T, Ra M, Taguchi R, Sakimura K, Mishina M (2010) Trans-synaptic interaction of GluR-delta2 and Neurexin through Cbln1 mediates synapse formation in the cerebellum. Cell 141:1068–1079. CrossRef Medline

Ullrich B, Ushkaryov YA, Südhof TC (1995) Cartography of neurexins: more than 1000 isoforms generated by alternative splicing and expressed in distinct subsets of neurons. Neuron 14:497–507. CrossRef Medline

Um JW, Pramanik G, Ko JS, Song MY, Lee D, Kim H, Park KS, Südhof TC, Tabuchi K, Ko J (2014) Calsyntenins function as synaptogenic adhesion molecules in concert with neurexins. Cell reports 6:1096–1109. CrossRef Medline

Vallee RB, Bloom GS (1991) Mechanisms of fast and slow axonal transport. Annu Rev Neurosci 14:59–92. CrossRef Medline

van de Bospoort R, Farina M, Schmitz SK, de Jong A, de Wit H, Verhage M, Toonen RF (2012) Munc13 controls the location and efficiency of dense-core vesicle release in neurons. J Cell Biol 199:883–891. CrossRef Medline

Vithlani M, Terunuma M, Moss SJ (2011) The dynamic modulation of GABA(A) receptor trafficking and its role in regulating the plasticity of inhibitory synapses. Physiol Rev 91:1009–1022. CrossRef Medline

Wittenmayer N, Körber C, Liu H, Kremer T, Varoqueaux F, Chapman ER, Brose N, Kuner T, Dresbach T (2009) Postsynaptic Neuroligin1 regulates presynaptic maturation. Proc Natl Acad Sci U S A 106:13564–13569. CrossRef Medline

Xue X, Jaulin F, Espenel C, Kreitzer G (2010) PH-domain-dependent selective transport of p75 by kinesin-3 family motors in non-polarized MDCK cells. J Cell Sci 123:1732–1741. CrossRef Medline

Zhai RG, Vardinon-Friedman H, Cases-Langhoff C, Becker B, Gundelfinger ED, Ziv NE, Garner CC (2001) Becausesembling the presynaptic active zone: a characterization of an active one precursor vesicle. Neuron 29: 131–143. CrossRef Medline

Zhang C, Atasoy D, Araç D, Yang X, Fucillo MV, Robison AJ, Ko J, Brunger AT, Südhof TC (2010) Neurexins physically and functionally interact with GABA(A) receptors. Neuron 66:403–416. CrossRef Medline

Zhang W, Rohlmann A, Sargsyan V, Aramuni G, Hammer RE, Südhof TC, Missler M (2005) Extracellular domains of alpha-neurexins participate in regulating synaptic transmission by selectively affecting N- and P/Q-type Ca2+ channels. J Neurosci 25:4330–4342. CrossRef Medline